Dear Etienne,

We would like to thank you and the reviewers for your time in reviewing our manuscript. We have carefully considered the reviewers' comments and have significantly revised our text as a result. In addition, we have added several supplementary figures, and believe these greatly strengthen the manuscript.

Please find our specific responses to each comment below.

Sincerely,

Josh Maurer, Summer Rupper, and Joerg Schaefer

Interactive comment on "Quantifying ice loss in the eastern Himalayas since 1974 using declassified spy satellite imagery" by Joshua M. Maurer et al.

T. Nuimura (Referee)

tnuimura@cis.ac.jp
Received and published: 9 May 2016

General comments

This manuscript addresses glacier variation over long period (1974–2006). The consistent procedure for generating DEMs use with HEXIMAP enables DEM differentiation with high accuracy, and overcomes procedure-dependent error. The estimated regional mass budget shows little discrepancy with previous studies. However, authors explanation about the discrepancy come from difference of analysed time span (previous studies only cover last decade) is reasonable.

Thank you for your thoughtful consideration of our manuscript. We have carefully considered your comments, and address all of them directly below.

Note: all page and line numbers refer to the final manuscript version (not the marked-up manuscript version with track changes).

Specific comments

P5 L9-10: Could you show the rate of estimated thickness change in each elevation band in Figure? For example, stack histogram in Fig. 4 might be better (extrapolated data with another color on blue histogram bar).

The rate of change is a simple scalar of the thickness change (i.e. thickness change divided by 32 years). We would like to keep this figure as simple as possible, and thus avoid adding extra

information in the elevation bands. Accordingly, we have left the figure as is, and instead notify the reader that in order to get the rate of change, values on the vertical axis can be divided by the timespan of 32 years.

To provide additional visualization of individual glacier changes and processing steps, we now include additional supplemental figures – 1) Fig S2 showing individual glacier profiles, and 2) Fig S3-S5 which show the processing steps for each glacier, including areas with interpolated data.

P6 L28: Does "standard error (SEM)" mean "standard error of the mean (SEM)" or "standard error (SE)"?

This was a typographical error, we have corrected it, and now state "standard error of the mean" on P7 L30.

P8 L12-13: The geodetic mass balance by Kääb et al. (2012) also includes East Nepal. Strictly speaking, elevation difference around Bhutan is more negative. In Gardelle et al. (2013), they re-calculated it as -0.52_0.16 in Table 5. The value should be used here.

We fixed this to show updated values from Table 5 in Gardell et al (2013) as suggested on P8 L30

P10 L13: Fig.4 is appropreate figure for checking summary of glacier variation tendency for each glacier type. However, such aggregation of each data make unclear each glacier characteristics. Is it possible to add ice thickness change profile of each glacier as colored lines into Fig.4? If it makes Fig. 4 ambiguous, please add it as another new figure.

A new figure (Figure S2) is now included in the supplement showing thickness changes for individual glaciers.

P10 L13–20: You have mentioned the three possibilities of the small lowering elevation bands (about 4600-4800 m) here. I recommend to investigate the reason by checking individual glaciers. Number of glaciers in these elevation bands (about 4600–4800 m) are 2 and 6 (from Fig. 4), so it is not laborious work. I guess your second possibility is correct.

As recommended, we carefully inspected the individual glaciers contributing to the lower elevation bins, using both Figure S2, the Hexagon and ASTER satellite imagery, as well as high resolution Google Earth imagery.

For clean-ice glaciers:

As noted in the text (and which can be seen in figure S2), glacier k is the dominant factor affecting the clean-ice profile in Figure 4. Since glacier k does not contribute to the lowest elevation bin, the bin exhibits an apparent smaller thickness change.

On closer inspection of glacier toes, we observe that several glacier toes appear darker toward their termini, which we interpret as increased amount of debris cover (glacier s and glacier o for example). The insulating effects of debris-cover likely contribute somewhat to the observed pattern, but based on our analysis, we conclude that the primary factor explaining this phenomenon is that glacier toes are thin to begin with, and thus have less ice to lose. Our 1974 glacier outlines include glacier toes which were already thin at that time, and we expect thinning from that point in time onwards to be smaller near the termini.

For debris-covered glaciers

Polygon glacier outlines have accuracy problems near debris-covered glacier toes. This is a well-known problem, as heavy debris-cover is indistinguishable from surrounding terrain. Unfortunately, without field measures of debris-thickness we find it impossible to back out the relative contributions of insulation effects vs. inaccurate glacier polygons at debris-covered glacier toes. However, we suggest that future work using SAR velocities may be able to address this problem.

For calving glaciers:

As mentioned in the text, meltwater is effectively stored adjacent to glacier termini in proglacial lakes, making the thickness change appear smaller due to the filling effect of the lake.

We have updated the text to better reflect these findings in section 4.3 on P11.

P11 L1–20: As I commented before, figure about ice thickness change profile for each glacier should be add. It make easy to understand discussion here.

We agree, and now include such a figure (Figure S2).

Figure 3: Description about elevation change for each glaciers (Glaciers a and b ...) should be moved to main text.

The discussion has been moved to main text as suggested.

typing errors

P9 L17, P15 L29: Correctly, his family name is notWatanbe butWatanabe. It is erratum by the journal 'Mountain Research and Development'.

Thank you, we have updated his family name.

Review TC-2016-48

General Comments

The potential of declassified optical stereo satellite imagery for glacier change detection is undisputed. Several studies quantified glacier volume changes using declassified Corona and Hexagon data, mainly focusing on small basins or individual glaciers only. For the processing nearly all of the studies used commercial software packages. From this point of view the study of Maurer is highly welcomed as it proposed an independent workflow for DEM generation. Moreover, the study of Maurer closes a gap of knowledge in terms of region-wide glacier mass balance investigations in Bhutan using declassified imagery.

The workflow of DEM generation has already been published in the ISPRS Journal of Photogrammetry and Remote Sensing (Maurer and Rupper, 2015). This paper builds upon this previous paper and presents an application in the field of glacier volume change assessment. All in all it is a nice paper and worth of prompt publishing.

Thank you for your positive comments on the approach and results. We also appreciate your careful consideration of the manuscript and your detailed comments/criticisms. We have carefully considered your comments, and address all of them directly below.

Note: all page and line numbers refer to the final manuscript version (not the marked-up manuscript version with track changes).

Specific Comments

P 3, L 29. How were the blocks selected? Were they defined with respect to the glacier extent?

Blocks were selected to maximize coverage of large glaciers across the region, and avoid regions with cloud cover. We have clarified this point in the text on P3, L30.

P 4, L2. “Points located on unstable terrain were excluded” – Based on ICIMOD glacier outlines?

The ICIMOD glacier outlines were used to exclude glacier terrain during optimization. The glacier outlines were first converted to a raster binary mask at the spatial resolution of the reference DEM used during optimization (SRTM in this case). Next, dilation (a morphological operation which adds pixels to edge boundaries) was used to slightly enlarge the glacier boundaries in the raster mask, which helped to eliminate any unstable glacier pixels not quite contained by the ICIMOD outlines, as well as possibly unstable moraines.

Additionally, in the optimization routine, any elevation change pixels outside of 3 standard deviations are excluded at each iteration, which effectively eliminates other unknown sources of large error during optimization.

We have updated the text in section 2.1 on P3-4 to more precisely explain our methods.

P 4, L 21. Hexigon -> Hexagon

Thank you for correcting this typographical error.

P 4, L 29. I am not familiar with glacier elevation changes in Bhutan. Comparing with the Everest Region 100 m seems to be suitable. However, the strong elevation change for glacier "k" and "i" might also justify a threshold of 150 or 200 m.

After checking thickness changes for the two glaciers with strongest changes (glaciers i and k), we find that for glacier i, the largest magnitude thickness change is -104 m (negative meaning the glacier has thinned), and only 24 pixels out of 6939 are more negative than -100 m (0.4%). For glacier k, the largest magnitude thickness change is -93 m, thus 0 pixels out of 57182 are more negative than -100. Given the uncertainties in the elevation change measurements, we find that the few excluded pixels in glacier i exhibiting thickness changes slightly more negative than -100 meters do not significantly affect results.

P 5, L 2. “Greatest accuracy” – What does it mean? Did you use a slope threshold to correct the outlines with regard to steep parts in the accumulation regions which have erroneously been delineated as part of the glacier? The delineation of debris-covered glacier tongues is often ambiguous. How did you cope with uncertainties in these regions (e.g. glacier “f” in Figure 3 shows a strong glacier thinning at the end of the tongue outside the glacier outline)?

At that time we inspected glacier polygon outlines from both the Randolph Glacier Inventory and ICIMOD. We found that polygons from the Randolph Glacier inventory had significant georeferencing errors in the Bhutan region, while those from ICIMOD appeared more detailed and accurate, based on visual inspection after overlying the outlines on high resolution Google Earth imagery. Recently these exact same ICIMOD outlines have been incorporated into the GLIMS database, but at that time they were not. We have updated the text on P5 L10.

As suggested, we have updated our workflow to include a slope threshold, to correct glacier areas by removing erroneously delineated parts (i.e nunataks, rock cliffs, etc.). We found that a threshold of 45 degrees was optimal, and have updated our results with this correction included. The text has also been updated on P5 L 13.

As noted in our uncertainties section, we expect relative vertical errors to occur between the Hexagon and ASTER DEMs, i.e. apparent elevation changes where no actual changes have occurred. This is due to different sensor characteristics, viewing geometries, sun position, cloud cover and atmospheric conditions, etc. between Hexagon and ASTER imagery. It is entirely possible these errors occur near a glacier toe, making it appear as though the change is part of the glacier, when in fact it is not. Further complicating this are actual non-ice elevation changes such a landslides and glacial-lake outburst floods, which can be triggered as glaciers recede and alter stress regimes along valley walls and moraine ridges, exposing unstable slopes, and reorganizing large volumes of unconsolidated sediment (e.g. Richardson, Shaun D., and John M. Reynolds. "An overview of glacial hazards in the Himalayas." Quaternary International 65 (2000): 31-47). Therefore, we base our glacier outlines primarily on the satellite imagery, with the thickness change maps as a secondary source. We also include a new supplementary figure, S6, which illustrates some unstable moraines which have since collapsed in the region, leading to non-ice elevation changes near glaciers. The associated text has been updated in the paragraph starting on P5 L16.

We agree regarding the common problem of ambiguous debris-covered glacier tongues. We have manually adjusted the ICIMOD glacier outlines to capture glacier extents to the best of our ability, however it is entirely possible (indeed likely) that some debris-covered toes are slightly inaccurate, as is the case for every previous study using remote sensing methods to study debris-covered glaciers. Unfortunately there is no foreseeable way of eliminating ambiguity regarding the separation of inaccurate glacier outlines, DEM errors, or reorganization of unconsolidated sediment, especially regarding glacier extents during the 1970's. We now discuss this problem in the text, and suggest a possible route for future studies to better delineate debris-covered glaciers (P5 L16).

P 5, L9-11. Data gaps in the accumulation regions are characteristic for DEMs generated using optical satellite imagery. Closing these gaps is indispensable for glacier mass balance calculations. Several approaches can be found in the literature, e.g. based on TINs (Surazakov and Aizen, 2006) or using the regional mean/median for individual elevation bands. Other studies assumed no change in the accumulation regions replacing missing data values by zero (Pieczonka and Bolch, 2013). Using the regional mean the authors assume a similar behavior for all glaciers of the same type. However, this must not necessarily be true. Taking this into account the proposed method allows the calculation of regional glacier volume changes but might not be suitable to calculate glacier volume changes for individual glaciers (e.g. P 10, L 4). Can you provide a difference image after extrapolation to judge the meaningfulness of the approach? You could also add a figure showing all three stages for an example glacier (difference image before hole interpolation, after hole interpolation, after extrapolation).

We now include results using both gap-filling methods (regional extrapolation for individual elevation bands and assuming zero change) in order to facilitate comparison in Table S3. In addition, 3 new supplementary figures are included which show each glacier at each processing stage (Fig S3-S5).

The text has been updated in the paragraph starting on P6 L3.

P 8, L12. The results from this study are not comparable to the results of Kääb et al. (2012) and Gardelle et al. (2013) due to different time periods. The authors should add other references when writing “is comparable to other estimates derived from remote sensing […]”. Compared to the Everest Region (Bolch et al., 2011) the regional mass budget is less negative. Zemp at al. (2009) give annual mass balances based on in-situ observations on a broader scale. For Southeast Asia they found a moderate mass loss until 1995 with a subsequent acceleration since 1996, reflecting the higher mass loss found by Kääb et al. (2009) and Gardelle et al. (2012) for the last decade.

We agree that the wording of this statement is inaccurate, as different time periods prevent direct comparison. The text has been updated accordingly in section 4.1 on P8-9, and results from the other studies mentioned have been added.

P 9, L 20. What is the source for the information regarding melt ponds? Did the authors use Google Earth for a visual inspection of the glaciers?

The source of the information was imagery viewed in Google Earth (updated on P10 L10).

P 10, L 15 and L 20. In my opinion it is a decrease from -35 to -10 m in line 15 and an increase from 0 to -10 m in line 20 as the values are related to glacier thinning.

We agree the wording was confusing, and have updated to more clearly describe the profiles in section 4.3 on P11.

P 11, L 7. “Low slope and low surface velocity” – This is imprecise and some further information is needed.

The statement has been updated to provide more information on P11 L33.

P 11, L 9. “Near stagnant flow velocities” – This statement is not supported by any figure or by a reference.

The reference to (Kaab, 2005) has been added on P12 L3.

P 11, L 14. “heavy debris” and “lighter debris” – What does it mean in terms of absolute debris thickness?

We mean that certain regions appear to have more or less area covered by debris, based on visual inspection of the satellite imagery. Darker = relatively more area covered by debris, lighter = relatively more area covered by ice.

The text has been updated to more precisely define our meaning on P12 L9.

Figure 2. 8 different Hexagon DEMs are mentioned. Figure 2 shows only 3 polygons. This needs to be changed to 8 polygons to get the link between Table S1 and Figure 2.

Labels for the 8 different Hexagon DEM regions have been added to Figure 2.

Figure 3. The chosen color for the investigated glaciers is unfavorable in comparison to the bright background color. A different color for the outlines would improve the readability of the figure significantly (in particular for the glaciers “q”-“u”).

We agree, and have changed the color of investigated glacier outlines from white to blue.

Figure 3. The current visualization using a continuous color coding shows an almost perfect fit between both models but conceals uncertainties in the data. The authors should use classes instead of a continuous color coding in order to allow a better distinction between areas of higher and lower deviations from zero, in particular for the stable terrain.

We now include a version of Figure 3 with classes in the supplement (Fig S7). However, we feel that a version with continuous color coding is essential for clearly illustrating the various spatial patterns of thinning with the most detail. Thus, we have retained the continuous version, but have improved it by enhancing the contrast to better highlight the elevation differences.

Figure 3. Glacier “a” shows a strong surface lowering in the middle part of the tongue followed by sudden elevation uplift at the end of the tongue. At the same time there is a strong thinning right next to the outline not mapped as a glacier.

On close inspection, we find a lateral moraine ridge has collapsed along the west margin of the glacier tongue, which likely caused the apparent elevation change there (Fig S6).

As Fig. S6 shows, the polygon does contain ice at the end of the tongue. We hypothesize that the apparent elevation uplift may be due to emergent velocities associated with glacier dynamics.

Figure 3. Considering glacier “k” and “i” I would expect a surface lowering of more than 100 m. The threshold of 100 m used to exclude outliers might be too low. A value of 150 or 200 m might be more suitable, in particular for the ablation regions. Can the author provide a difference image before gap interpolation in the supplements?

See previous comment regarding P4, L 29. We also now include Figs S3-S5 to show difference images at various stages, including before and after gap interpolation.

Table S2. Area uncertainties for 1974 are missing.

The area uncertainties have been added.

Interactive comment on "Quantifying ice loss in the eastern Himalayas since 1974 using declassified spy satellite imagery" by Joshua M. Maurer et al.

J.M. Shea (Referee)
joseph.shea@icimod.org
Received and published: 23 May 2016

Using declassified spy satellite imagery (Hexagon and Corona) and recent ASTER imagery, Maurer et al calculate glacier mass changes for 21 glaciers in eastern Bhutan, from the 1974 to 2006. The methods and assumptions appear to be sufficient, errors in the analysis are well-documented, and the results are interesting and highly relevant. The paper is also well-referenced, very well-written, and essentially free from grammatical/structural/organizational errors.

Thank you for your helpful comments on the manuscript. We have addressed all of your concerns below, and feel they have improved the paper considerably.

Note: all page and line numbers refer to the final manuscript version (not the marked-up manuscript version with track changes).

Aside from the comments by the other reviewers (Pieczonka and Nuimura), I can only add a few general points that the authors might wish to address:

1) A very brief outline of the Hexagon/Corona pipeline (Maurer and Rupper, 2015) would be helpful.

We now include a brief summary of the process in section 2.1 on P4.

2) Why are only 21 glaciers studied? And what are the impacts of the 30% coverage threshold? Previous geodetic studies (e.g. Gardelle et al., 2013, Bolch et al., 2011) consider the entire glacierized area that is covered within a region. Using only 21 glaciers (and only those larger than 3 km2) and replacing potentially large missing areas with the regional mean for a specific glacier type and elevation band could result in biased regional estimates of glacier mass change that are not comparable to previous studies.

In short, low radiometric contrast, cloud cover, and spatially correlated noise/error in the DEMs prevent accurate calculation of changes for all glaciers in the region. While this does limit direct comparison to other previous studies (this among other things, such as different timespans covered), we feel these 21 large glaciers give a good regional picture of thickness changes over the 3 decade timespan. We have updated the discussion to more accurately reflect these facts in the paragraph starting on P6 line 14.

3) How is the ELA defined in this study (it first appears on P10L29)? Strictly speaking, this is typically taken from surface mass balance measurements. While the elevation that divides geodetic mass gain and loss would be related to the ELA, I am not sure that it can be used as an ELA substitute (though I would be interested to hear otherwise).

We agree the term "ELA" was being used too loosely here, and instead substitute the term "glacier hypsometry." Updated on P11 L20.

Specific comments:

P2L20: are these annual or seasonal streamflow contributions?

These are seasonal, their samples (from which their streamflow contributions were derived) were collected during September (post-monsoon). We have updated the text to make this important distinction clear (nice catch by the reviewer).

The text has been updated on P2 L19.

P4L20: Define DN.

DN = Digital Numbers, these are simply the pixel values in Landsat and ASTER images before being converted to reflectance or radiance. Updated on P4 L28.

P10L25: What data support the conclusion that debris-covered glaciers melt at the same rate as clean-ice glaciers? If this is overall mass balance rates than it should be specified. Figure 4 clearly shows that melt rates at debris-covered glaciers are lower than those observed on clean ice glaciers for the same elevation band, and this is later referenced by the authors on P10L28.

We now clarify at the beginning of the section, that although elevation distributions of ice loss differ between clean-ice and debris-covered glacier groups, overall geodetic mass balance values are similar in magnitude. Updated on P11 L16.

P11L15: Debris cover will almost always get thinner moving up-glacier. The greater thinning rates observed at the transition between debris-covered and debris-free zones is due in part to enhanced melt rates under thin debris cover but also due to the simple fact that bare ice will melt at a faster rate than debris-covered ice at the same elevation. Modelling studies in the Khumbu region (Shea et al., 2015; Rowan et al., 2015) both indicate that debris-covered tongues will detach from their accumulation areas in the future, leading to greater future melt rates.

We agree, and now include this statement and accompanying references in the text on P12 L12.

Quantifying ice loss in the eastern Himalayas since 1974 using declassified spy satellite imagery

Joshua M. Maurer[1,2], Summer B. Rupper[3], Joerg M. Schaefer[1,2]

[1]Lamont-Doherty Earth Observatory (L-DEO), Palisades, NY 10964, USA
[2]Department of Earth and Environmental Sciences, Columbia University, New York, New York 10027, USA
[3]University of Utah, Department of Geography, Salt Lake City, UT 84112, USA

Correspondence to: Joshua M. Maurer (jmaurer@ldeo.columbia.edu)

Abstract. Himalayan glaciers are important natural resources and climate indicators for densely populated regions in Asia. Remote sensing methods are vital for evaluating glacier response to changing climate over the vast and rugged Himalayan region; yet many platforms capable of glacier mass balance quantification are somewhat temporally limited considering typical glacier response times. We here rely on declassified spy satellite imagery and ASTER data to quantify surface lowering, ice volume change, and geodetic mass balance during 1974-2006 for glaciers in the eastern Himalayas, centered on the Bhutan-China border. The wide range of glacier types allows for the first mass balance comparison between clean, debris, and lake-terminating (calving) glaciers in the region. Measured glaciers show significant ice loss, with an estimated mean annual geodetic mass balance of -0.132 ± 0.06 m.w.e. yr^{-1} (meters of water equivalent per year) for 10 clean-ice glaciers, -0.~~15~~ 19 ± 0.11 m.w.e. yr^{-1} for 5 debris-covered glaciers, -0.285 ± 0.10 m.w.e. yr^{-1} for 6 calving glaciers, and -0.176 ± 0.05 m.w.e. yr^{-1} for all glaciers combined. Contrasting hypsometries along with melt pond, ice cliff, and englacial conduit mechanisms result in statistically similar mass balance values for both clean-ice and debris-covered glacier groups~~The similar mass balances for clean-ice and debris-covered glaciers suggests that melt pond, ice cliff, and englacial conduit mechanisms are likely playing important roles in the melt process for debris-covered glaciers.~~ . Calving glaciers comprise 1824% (6680 km^2) of the glacierized area, yet have contributed 307% (-0.7 km^3) to the total ice volume loss, highlighting the growing relevance of proglacial lake formation and associated calving for the future ice mass budget of the Himalayas as the number and size of glacial lakes increase.

Commented [J1]: Updated processing procedures (see section 2.3) now result in moderately different numbers here. Excluding steep non-glacial terrain in the accumulation zones (see page 5 line 25) had the largest effect on the mass balance value reported for debris-covered glaciers. However, these moderate changes do not affect the conclusions of the paper.

Commented [J2]: See comments on page 9 lines 10-17

1 Introduction

Glaciers in high mountain Asia hold the largest store of ice outside the Polar Regions and contribute meltwater used by roughly 20 percent of the world's population for agriculture, energy production, and potable water (Immerzeel et al, 2010). Glacier changes must be quantified in order to evaluate impacts to hydrology and ecosystems, assess glacial lake outburst flood (GLOF) hazards, calculate recent contributions to sea level rise, and increase predictive capabilities regarding future change and resulting impacts.

The heterogeneity of Himalayan glaciers poses significant challenges in quantifying and modelling glacier changes. Debris-cover in the ablation zone and calving in proglacial lakes are particularly noteworthy examples of complicating factors that may significantly affect the response of many glaciers. Bolch et al (2012) estimate the proportion of debris-covered ice in the Himalayas is ~10%, and Scherler et al (2011) estimate that 93% of glaciers in the Himalayas have > 20% debris-covered areas. Debris-covered glaciers are difficult to model, since debris can either increase or suppress melt depending on debris thickness and extent, though debris-covered glaciers in the Himalayas are mostly assumed to be less responsive to ongoing warming (Scherler et al, 2011). Similarly, numerical models of glaciers terminating in moraine-dammed proglacial lakes are poorly constrained, and these glaciers can undergo enhanced ice loss through calving and thermal-undercutting processes independent of climate. Lake-terminating glaciers have particular societal relevance, because the growing lakes can cause GLOFs (Glacial Lake Outburst Floods), as well as impact glacier mass balance and hydrology.

Response of Himalayan glaciers to changing climate remains somewhat controversial, primarily due to this complexity of the glacier systems combined with scarcity of direct observation, and no unambiguous pattern has emerged (Berthier et al, 2007; Kääb et al, 2012). Complex politics, rugged terrain, and the immense number of glaciers result in a severe lack of field data (Bolch et al, 2011; Rupper et al, 2012)~~(Bolch et al, 2011; Rupper et al, 2012)~~. The few available field records in the Himalayas are often biased towards small to medium-sized clean-ice glaciers due to logistical reasons (Gardelle et al, 2013). Thus there is a critical need for spatially and temporally extensive glacier change data that captures the full spread of glacier complexities over timespans relevant to glacier response times.

Here we focus on the eastern monsoonal Himalayas, centered on the Bhutan-China border. Few data on glacier changes are available and the region has a large diversity of glaciers with regard to elevation, size, debris-cover, hypsometry, accumulation rates and calving characteristics. Furthermore, glacier meltwater is an important hydrological resource in Bhutan, including for hydroelectric power generation (Beldring and VoksØ, 2012). Recent hydrologic mixing model results using isotopic and geochemical chemistry have estimated glacier seasonal outflow contributions to the Chamkar Chhu river in Bhutan ranging from ~76% at 4500 m to 31% at 3100 m elevation duing September (post-monsoon) (Williams et al, 2015).

There are several clean glaciers flowing northward onto the Tibetan Plateau with high velocities, likely with large amounts of basal sliding (Kääb, 2005). On the southern flank, most large glaciers are debris-covered, located in steep valleys, and show slow-to-nearly stagnant velocities, with many depressions and melt pond features. Additionally, ~~numerous~~ several glaciers (including clean and debris-covered) terminate in moraine-dammed lakes. The majority of clean-ice glaciers in the Bhutan-centered region have a high mass turnover, with most accumulation and ablation occurring during the summer months as a result of the Indian monsoon (Rupper et al, 2012). In regions with high accumulation, ablation is dominated by melt and thus particularly sensitive to changes in temperature (Rupper and Roe, 2008). Robust melt models indicate these eastern-Himalayan, temperature-sensitive glaciers are currently out of balance with present climatology. One estimate predicts a loss of almost 10% of the current glacierized area, with an associated drop in meltwater flux of as much as 30%

within the next few decades (Rupper et al, 2012). Kääb et al. (2012) computed a 2003-2008 specific mass balance of -0.26 ± 0.07 to -0.34 ± 0.08 m.w.e. yr^{-1} (depending on different density scenarios for snow and ice) for eastern Nepal and Bhutan using laser altimetry, while Gardelle et al. (2013) estimated a 1999-2011 geodetic mass balance of −0.22 ± 0.12 m.w.e. $yr^{-1}$for Bhutan by differencing SPOT5 and SRTM DEMs (digital elevation models). Another recent study utilizing multi-temporal Landsat images to compute glacier area changes in Bhutan showed 23.3 ± 0.9% glacial area loss between 1980 and 2010, with loss mostly observed below 5600 m a.s.l., and greater area loss for clean glaciers (Bajracharya et al, 2014). The first decadal mass-balance record of the Gangju La glacier in the Bhutan Himalaya was recently published, in which a mass balance of –1.12 to –2.04 m.w.e. yr^{-1} was estimated between 2003 and 2014 (Tshering and Fujita, 2015).

To build on these pioneering studies and further constrain glacier changes, we utilize a new pipeline (Maurer and Rupper, 2015) to extract DEMs from declassified Hexagon imagery (1974) and ASTER scenes (2006), then use DEM differencing to measure ice volume change and geodetic mass balance between 1974 and 2006 in this temperature-sensitive, monsoon-influenced region. Our approach provides high spatial detail and longer temporal range compared to previous measurements, and circumvents significant uncertainties regarding SRTM radar penetration in ice and snow (Gardelle et al, 2012).

2 Methods

Previous studies have demonstrated the value of declassified spy satellite imagery for glacier mass and volume change quantification in various regions of the Himalayas (Lamsal et al, 2011; Bolch et al, 2011; Pieczonka et al, 2013; Bhambri et al, 2013; Raj et al, 2013; Racoviteanu et al, 2014; Pieczonka and Bolch, 2015; Holzer et al, 2015; Pellicciotti et al, 2015; Ragettli et al, 2016)~~(Lamsal et al, 2011; Bolch et al, 2011; Pieczonka et al, 2013; Bhambri et al, 2013; Raj et al, 2013; Racoviteanu et al, 2014; Pieczonka and Bolch, 2015; Holzer et al, 2015; Pellicciotti et al, 2015; Ragettli et al, 2016)~~. We rely here on a new workflow called HEXIMAP (Hexagon Imagery Automated Pipeline) which utilizes computer vision ~~techniques~~ algorithms to extract DEMs with high efficiency and accuracy (Maurer and Rupper, 2015). Both Hexagon and ASTER DEMs are extracted using similar methods in order to minimize unwanted elevation bias caused by different image processing techniques. The resulting elevation change maps are used to compute average surface lowering of glaciers, changes in ice volume, and geodetic mass balance.

2.1 Hexagon

The Hexagon program consisted of a series of 20 photographic reconnaissance satellite systems developed and launched by the United States, operational from 1971 to 1986 during the Cold War era. Each satellite carried approximately 96.5 km of film, and thousands of photographs worldwide were acquired using the mapping camera system (ground resolution of 9 meters, improved to 6 in later missions). The Hexagon mapping camera system acquired multiple 3400 km^2 frames as the satellite proceeded along its orbital trajectory. After image acquisition, film-recovery capsules were ejected from the

satellite and parachuted back to earth over the Pacific Ocean, where they were retrieved midair via "air snatch" by C-130 Air Force planes. The images have overlap of approximately 55 to 70%, which allows for extraction of digital elevation models (Oder et al, 2012; Surazakov and Aizen, 2010).

Eight separate 5000 x 5000 pixel blocks ~~are~~ are processed, which correspond to approximately 20 x 20 km regions with the Hexagon film scanned at 7 µm resolution (orange outlines in Fig. 2), with blocks selected to maximize coverage of glaciers and avoid regions with cloud cover. The same HEXIMAP (Hexagon Imagery Automated Pipeline) methodology, outlined in Maurer and Rupper (2015) is used to extract Hexagon DEMs. ~~regarding stereo rectification, computation of disparity maps, and nonlinear optimization of the position and global scale of each Hexagon DEM to match the SRTM 1 arc-sec global DEM.~~In summary, epipolar images are generated by computing homography transformations via automated point detectors and descriptors (Bay et al, 2006; Fusiello and Irsara, 2008). After epipolar resampling, image features line up horizontally and the disparity search is reduced to one horizontal dimension. Disparity maps are computed using the semi-global block matching algorithm (Hirschmüller, 2008), bundle adjustments are performed to minimize reprojection error, and stereo-matched points are triangulated in 3D space using the direct linear method (Hartley and Zisserman, 2003). The 3D point clouds are registered to the reference SRTM DEM using nonlinear optimization of pose parameters including rotation, translation, and a global scale factor. ~~Points located on unstable terrain (e.g. glaciers) are excluded during optimization.~~ ICIMOD glacier outlines are utilized to exclude glacial terrain during optimization (after being manually edited to match the glacier extent in 1974). The glacier outlines are first converted to a raster binary mask to match the spatial resolution of the reference DEM. Next, dilation (a morphological operation which adds pixels to edge boundaries) is performed to slightly enlarge the glacier boundaries in the raster mask, which helps to eliminate unstable glacier pixels not contained by the glacier outlines, as well as eliminate possibly unstable moraines (see Fig S6). Any elevation change pixels outside of 3 standard deviations are excluded during each iteration in the optimization routine, which effectively eliminates other unknown sources of error during optimization.The higher spatial-resolution Hexagon point clouds are then resampled to match ASTER data (~30 m intervals) using linear interpolation. Data voids larger than ~~i~~$_{h}$ 2 km^2 ~~(see Table S1, footnote 4)~~ are not interpolated to avoid biasing glacier change results with unrealistic terrain (Fig. S3-S5). ~~Lastly, the DEMs are post-processed using a 5x5 median filter and an edge-preserving mesh denoising algorithm (Sun et al, 2007).~~

Formatted: Superscript

Commented [J3]: In our updated workflow, we forgo this final step, because it is somewhat unnecessary and does not affect results significantly.

2.2 ASTER

The Advanced Spaceborne Thermal Emission and Reflection Radiometer (ASTER) was launched on board NASA's Terra spacecraft in December, 1999 as part of a cooperative effort between NASA and Japan's Ministry of Economic Trade Industry (METI). In the visible and near-infrared (VNIR) spectral region (0.78-0.86 µm), ASTER has a nadir view telescope as well as a backward looking telescope to provide stereoscopic capability at 15m ground resolution. Both use 4000 element charge-coupled detectors (CCD's), acquiring data via linear pushbroom scanning. Each ASTER scene covers approximately 60 x 60 km (Abrams, 2000). Although a global ASTER DEM (GDEM v2) is publicly available, anomalies and artifacts in the data limit its utility for glacier change quantification. Instead, two ASTER Level-1A scenes (granule ID: ASTL1A

06120404462306120703 03 and ASTL1A 06020304454106020603 03) were downloaded from the GDS (Ground Data Systems) ASTER/PALSAR Unified Search website, maintained by Japan Space Systems. DEMs were extracted from the scenes using similar methodology as previously described for the Hexagon imagery, with a few key differences. First, ~~raw~~ DN (digital number) pixel values from the VNIR images are converted to radiance and processed to remove residual striping artifacts. Second, since ASTER images are acquired by a linear pushbroom sensor they do not have a single fixed center of perspective (Kim, 2000). Consequently, epipolar images cannot be generated using a single homography transformation as was done with Hexa~~i~~gon images. Alternatively, sight vectors and satellite position matrices (supplied with ASTER ephemeris data) for each CCD row are used to project ASTER forward and backward looking images to a common image plane, after which corresponding pixels in the stereo images are matched using the same stereo-matching algorithm in HEXIMAP. Lastly, point clouds are triangulated by computing sight vector intersections in 3D space rather than using the direct linear method. All other aspects regarding DEM extraction are identical to the Hexagon methodology, thus minimizing any unwanted potential elevation bias caused by different image processing techniques.

2.3 Geomorphic Change

To compute glacier changes, the 1974 Hexagon DEMs are subtracted from the 2006 ASTER DEMs to create elevation change maps. Pixels located in areas with > 30° slope are excluded from analysis due to lower accuracies during the DEM extraction process ~~located in areas with > 30° slope, > 0.07 m^{-1} maximum surface curvature, and < 2 neighborhood pixel standard deviation (a measure of local image contrast) are excluded from analysis due to lower accuracies during the DEM extraction process~~ (Maurer and Rupper, 2015). ~~Any e~~Elevation changes over 100 meters ~~are~~ are ~~also excluded, as changes this large are~~ likely due to stereo matching errors from ~~shadows,~~ cloud cover or low radiometric contrast,~~, e~~ and are thus also excluded. ~~te. Small holes are interpolated (Table S1) before statistical analysis.~~ To delineate glacier boundaries, polygons representing glacier outlines were downloaded from the ICIMOD mountain geoportal (http://geoportal.icimod.org/), which were found to have comparatively ~~the~~ greate~~r~~st detail and accuracy for this region compared to the Randolph Glacier Inventory, based on overlay and visual inspection of Google Earth imagery. The polygons were then manually edited to reflect ~~glacier~~ the spatial ~~outlines~~ extent of glaciers in 1974 and 2006 based on visual interpretation of the Hexagon and ASTER imagery, along with examination of the elevation change maps. We also use a slope threshold of 45° to exclude any steep parts (nunataks and rock cliffs) in accumulation regions which were erroneously delineated as part of a glacier and update the glacier outlines accordingly.

Relative vertical errors between the Hexagon and ASTER DEMs are expected due to different sensor characteristics such as viewing geometry, sun position, cloud cover, and atmospheric conditions. Further complicating this are non-ice geomorphic changes such as landslides, which can be triggered as glaciers recede and alter stress regimes along valley walls and moraine ridges, exposing unstable slopes, and reorganizing large volumes of unconsolidated sediment (Richardson and Reynolds, 2000). Several collapsed moraines were observed in the region (Fig. S6), therefore we base our clean-ice and calving glacier outlines primarily on visible satellite imagery, with the thickness change maps as a secondary source. On the

Commented [J4]: This section describes our updated (post-review) workflow.

Formatted: Indent: First line: 0.25"

other hand, we base our debris-covered glacier outlines primarily on the thickness change maps, as debris covered glaciers are difficult to distinguish from surrounding terrain using visible imagery only. Future work could focus on utilizing alternate methods to delineate these glaciers, such as using SAR velocities to detect slowly moving ice (Mattar et al, 1998; Strozzi et al, 2002).

Glacier elevation models extracted using stereo photogrammetry often have errors and ~~data~~ gaps over snow-covered accumulation zones due to low radiometric contrast and sensor oversaturation (Pellikka and Rees, 2009). Hexagon film strips are especially vulnerable to this problem, resulting in large regions of missing data ~~,~~ and some apparently erratic thickness changes over ~~,~~ glacier accumulation zones ~~(Fig. 3)~~. To ~~In order to avoid unrealistic surfaces which can significantly bias results, HEXIMAP does not perform automated interpolation schemes~~ exclude these ~~over these regions~~erroneous regions, we compute the neighborhood standard deviation of each image pixel (a measure of local image contrast, using a 5x5 window), along with the gradient and curvature of the thickness change map for each glacier. Pixels with neighborhood standard deviations less than 3, which also have either a thickness change gradient > 45, or a curvature value > 0.005 m^{-1} are excluded, and gaps in the thickness change maps smaller than 2 km^2 are interpolated (Fig. S3-S5). This method allows for removal of erroneous pixels in low-contrast accumulation zones, while retaining pixels in debris-covered zones which often have greater local gradient and curvature values due to melt ponds and ice cliffs.

To close remaining data gaps in accumulation regions, various approaches can be found in the literature. Gardelle et al (2013) replace missing thickness change data over glaciers by the regional mean of the corresponding elevation band for a given glacier type, based on the assumption that thickness changes should be similar at a given altitude across the region. Pieczonka and Bolch (2013) assume no change in the accumulation regions and replace missing data values by zero. ~~. In this study, missing thickness change data over glaciers are replaced by the regional mean of the corresponding elevation band for a given glacier type (Fig. 4); based on the assumption that thickness changes should be similar at a given altitude across the region (Gardelle et al, 2013). Missing data for different glacier types are extrapolated using the corresponding thickness change profiles (either clean, debris, or calving).~~Due to the spatially heterogeneous nature of glacier changes in Bhutan, and the limited number of contributing pixels at high elevation bands (Fig. 4), the regional extrapolation method introduces significant bias, especially regarding the large region of missing data in the accumulation zone of glacier c. Thus, all regional glacier change values reported in the text are derived using the method which assumes zero change for missing data. To examine the effect on geodetic mass balance and facilitate a comparison between the two methods, we also include separate results derived using each assumption (replacing missing data with zero change vs. regional extrapolation) in Table S3. For the extrapolation method, missing data for different glacier types are extrapolated using the corresponding thickness change profiles (either clean, debris, or calving).

A total of 21 glaciers are selected (Fig. 2, outlined in white) based on size (glaciers larger than 3 km^2), and data coverage (glaciers with at least ~~30~~25% glacier area covered by the DEMs). Unfortunately, .incomplete coverage of remote sensing data, clouds, and poor radiometric contrast in some areas prevent accurate investigation of all glaciers. While this

Formatted: Superscript

Formatted: Superscript

does limit direct comparison to other previous studies which may measure all glaciers in a region, these 21 largest glaciers give a good regional picture of thickness changes over the 3 decade timespan.

Debris-covered areas for each glacier are delineated using a Landsat TM4/TM5 DN band ratio image with a threshold of 2.0 (Paul, 2000). Non-calving glaciers with 20% or greater debris-covered area are assigned the debris category (5 glaciers); non-calving glaciers with less than 20% are assigned the clean category (10 glaciers). The calving category (6 glaciers) includes both clean and debris types which terminate in lakes as determined by viewing the Hexagon and ASTER imagery.

For each glacier, the ice volume change, spatially-averaged thickness change, and geodetic mass balance over the 32-year timespan are computed using the elevation change maps following Eq. (1-3):

$$\Delta \boldsymbol{V} = \sum_{i=1}^{n} \boldsymbol{D_i r^2}, \quad (1)$$

$$\bar{\boldsymbol{h}} = \frac{\Delta \boldsymbol{V}}{\boldsymbol{A}}, \quad (2)$$

$$\dot{\boldsymbol{b}} = \bar{\boldsymbol{h}} \boldsymbol{\rho}, \quad (3)$$

where ΔV is ice volume change (m^3), D_i is the elevation change (m) for pixel i located within a glacier polygon, n is the total number of pixels within a glacier polygon, r is the resolution of the elevation change map (~30 m), $\bar{h}$ is the spatially-averaged elevation change of the glacier, A is the average of the 1974 and 2006 glacier areas (m^2), $\dot{b}$ is the geodetic (specific) mass balance, and ρ is the estimated average density of glacier ice; here we use an intermediate value between firn and ice of 850 ± 60 kg/m^3 as recommended by Huss (2013). Geodetic mass balance values are converted to m.w.e. (meters water equivalent) by dividing $\dot{b}$ by the density of water (1000 kg/m^3).

2.4 Relative accuracy between DEMs and glacier change uncertainties

Statistical significance of elevation changes are quantified by estimating the relative vertical accuracy between the Hexagon and ASTER DEMs. Table S1 shows the root-mean-square error, mean, median, normalized median absolute deviation, standard deviation, 68.3% quantile, and 95% quantile of elevation changes between each approximately 20 by 20 km Hexagon DEM (orange outlines in Fig. 2) and the ASTER DEM (blue outline in Fig. 2) for assumed stable (ice-free) terrain. Plots of elevation change against elevation, slope, curvature, ASTER along-track and cross-track were also examined for potential biases (Fig. S1). We neglect any global corrections, as the vast majority of data lie in regions with close to zero bias, and pixels with ~~extreme curvature (> 0.07 m^{-1}) and~~ high slope (> 30°) are excluded as outlined in section 2.3.

To assess uncertainties for glacier changes, the point elevation error (E_{pt}) and extrapolation error (E_{ext}) are used to calculate the total elevation error (E_z) for a given elevation band (Nuth et al, 2010):

$$\boldsymbol{E_z} = \sqrt{\left(\frac{\boldsymbol{E_{pt}}}{\sqrt{\boldsymbol{n_z}}}\right)^2 + \left(\frac{\boldsymbol{E_{ext}}}{\sqrt{\boldsymbol{n_z}}}\right)^2}, \quad (4)$$

The standard deviations of the relative elevation change over stable terrain are used for E_{pt} (Table S1), while the standard deviations of glacial elevation change within each 100 m elevation band are used as approximations for E_{ext}. These E_{ext}

estimates are conservative because the elevation bands contain intrinsic natural variability, as not all glaciers have undergone the same elevation change at a given elevation (Gardelle et al, 2013). The n_z value represent the number of independent pixel measurements. To account for spatial autocorrelation, we estimate n_z as:

$$\boldsymbol{n_z = \frac{n_b * r^2}{\pi * d^2}}, \quad (5)$$

where n_b is the number of pixels in a given glacier elevation band, r is the pixel resolution (~ 30 m), and d is the distance of spatial autocorrelation (Nuth et al, 2010; Nuth and Kääb, 2011). For glacier regions where data exists (i.e. covered by an elevation change map, thus no extrapolation is necessary), E_{ext} is set to zero and the numerator in Eq. 5 is set to the ~~continuous~~ area within the glacier covered by elevation change data. To estimate d, we perform a semivariogram analysis, which relates variance to sampling lag and gives a picture of the spatial dependence of each data point on its neighbour (Curran, 1988; Rolstad et al, 2009). For all eight regions, we find the range varies from approximately 300 to 450 m, and thus choose a conservative value of 500 m for d. The volume change error for a given glacier is then estimated as:

$$\boldsymbol{E_{vol} = \sqrt{\sum_1^z (E_z * A_z)^2}}, \quad (6)$$

where A_z is the area of the glacier within a given elevation band Z. E_{vol} is then combined with glacier area uncertainties of ± 10% and an ice density uncertainty of ± 60 kg/m^3 using standard quadratic (uncorrelated) error propagation. All final glacier change uncertainties are reported as ± 1 ~~standard error (SEM)~~SEM (standard error of the mean) unless noted otherwise.

3 Results

Probability density plots of regional elevation change between the years 1974-2006 yield a negatively-skewed distribution for glaciers with a mean of -11 m and a standard deviation of 20 m, reflecting the approximate span of ice surface lowering. The surrounding ice-free terrain shows a more narrow distribution centered near zero, with a mean of 0.7 m and a standard deviation of 10 m (Fig. 1). Non-zero elevation change values in the ice-free terrain distribution (blue region, Fig. 1) are likely caused by a combination of actual changes such as landslides, errors caused by clouds, and other intrinsic errors associated with stereo photogrammetric methods used to create the DEMs.

All clean, debris, and calving glaciers investigated here for change during the 32-year timespan show predominate lowering and retreat of ice surfaces (Figs. 2 and 3). Individual glacier change statistics are also given in Table S2, including ice volume changes ~~(before and after extrapolation of missing data)~~, spatially averaged thickness changes ~~(after extrapolation)~~, and geodetic mass balances ~~over the 32-year timespan (after extrapolation).~~.

The relatively consistent negative mass balance trend includes both clean and debris-covered glaciers. Further insight into the ice-loss patterns can be obtained by examining the elevation change maps (Fig. 3). Most clean glaciers are retreating and exhibit thinning near their toes. Conversely, the debris-covered glaciers exhibit irregular patterns of elevation loss in their ablation area. Several smaller debris-covered glaciers have varying amounts and distributions of debris, and show different patterns of thinning. Some glaciers show the greatest thinning near their toes, others exhibit downwasting in mid-

section of the glacier, and still others display scattered ice-loss features. Ice loss is greatly enhanced for several glacier toes terminating in moraine-dammed lakes.

~~In estimating the regional mass balance, glacier c is problematic due to a lack of thickness change data across its very large, high accumulation zone (Fig. 3). The regional clean-ice glacier profile is also somewhat unreliable at these very high elevation bands due to the limited number of contributing pixels (Fig. 4). Due to its large size relative to the other glaciers, extrapolating across this entire region likely introduces significant unrealistic bias which overshadows the measured ice thickness changes of other glaciers. To avoid this potential large source of error, glacier c is excluded in the regional mass balance estimates and also excluded from relative contributions of clean-ice, debris-covered, and calving glaciers discussed in the following sections. Results obtained both with and without glacier c can be found in the supplement (Table S3).~~

~~The mean (area-weighted) geodetic mass balance for the selected glaciers (Fig. 2, outlined in white, excluding glacier c) is estimated to be -5.1 ± 2.2 m.w.e. for the period 1974 to 2006. Averaged over the 32-year timespan, this yields an annual mass balance of -0.16 ± 0.05 m.w.e. yr^{-1}. Clean glaciers comprise 47% (152 ± 15 km^2) of the total studied glacierized area (327 ± 32 km^2 for 21 glaciers), and have contributed 36% (-0.71 ± 0.33 km^3) to the total ice volume loss with a mass balance of -0.12 ± 0.06 m.w.e. yr^{-1}. The debris glaciers comprise 29% (96 ± 10 km^2) of the total glacierized area, and have contributed 27% (-0.53 ± 0.40 km^3) to the total ice volume loss with a mass balance of -0.15 ± 0.11 m.w.e. yr^{-1}. Calving glaciers comprise 24% (79 ± 8 km^2) of the total glacierized area, and have contributed 37% (-0.74 ± 0.28 km^3) to the total ice volume loss with a mass balance of -0.25 ± 0.10 m.w.e. yr^{-1}.~~

The mean (area-weighted) geodetic mass balance for the selected glaciers (Fig. 2, outlined in ~~white, excluding glacier c~~blue) is estimated to be -5.4 ± 1.6 m.w.e. for the period 1974 to 2006. Averaged over the 32-year timespan, this yields an annual mass balance of -0.17 ± 0.05 m.w.e. yr^{-1}. Clean glaciers comprise 61% (221 ± 11 km^2) of the total studied glacierized area (365 ± 12 km^2 for 21 glaciers), and have contributed 46% (1.09 ± 0.4 km^3) to the total ice volume loss with a mass balance of -0.13 ± 0.06 m.w.e. yr^{-1}. The debris glaciers comprise 21% (78 ± 4 km^2) of the total glacierized area, and have contributed 24% (-0.55 ± 0.4 km^3) to the total ice volume loss with a mass balance of -0.19 ± 0.11 m.w.e. yr^{-1}. Calving glaciers comprise 18% (66 ± 3 km^2) of the total glacierized area, and have contributed 30% (-0.70 ± 0.3 km^3) to the total ice volume loss with a mass balance of -0.28 ± 0.10 m.w.e. yr^{-1}.

Commented [J5]: The values reported in this paragraph are the result, after using the updated methodology described in section 2.3.

4 Discussion

4.1 Regional Glacier Change

The regional mass budget result of -0.~~16~~ 17 ± 0.05 m.w.e. yr^{-1} from 1974-2006 is ~~comparable to~~less negative than other estimates derived from remote sensing over shorter time periods. For example, ~~In particular, Kääb et al (2012) report a geodetic mass balance of -0.26 ± 0.07 or -0.34 ± 0.08 m.w.e. yr^{-1} depending on different density scenarios for snow and ice, and~~ Gardelle et al. (2013) ~~show~~ reported a mass budget of -0.22 ± 0.12 m.w.e. yr^{-1} ~~from~~ during 1999-2011 ~~for Bhutan~~, and recalculated the Kääb et al (2012) results to obtain -0.52 ± 0.16 m.w.e. yr^{-1} during 2003-2008 for the Bhutan region.

Additionally, our estimate is significantly less negative compared to the 1970-2007 mass budget of 0.32 ± 0.08 m w.e. a^{-1} in the neighbouring Everest region estimated by Bolch (2011). We hypothesize that the shorter more recent timespans of the Kääb et al (2012) and Gardelle et al (2013) studies result in more negative mass budgets due to accelerating glacier retreat in Asia since the end of the 1970's (Zemp et al, 2009). Addition influencing factors include different spatial extents covered, radar penetration uncertainties involved with SRTM data (not an issue in this study), and different methods of dealing with data gaps in accumulation zones.

Table S3 gives results obtained using the two different gap-filling methods in accumulation zones. Both methods yield similar geodetic mass balance values when glacier c (which has a disproportionately large region of missing data at high elevation) is not extrapolated, and purely by chance add up to exactly similar values for ΔV and $\dot{b}$ in the "all" category. When glacier c is extrapolated using the limited number of contributing pixels at high elevation, it introduces significant unrealistic bias which overshadows the measured ice thickness changes of other glaciers, making the regional mass balance values unrealistically positive. This illustrates that care must be taken when extrapolating from individual elevation bands from regional profiles, to avoid extrapolating large regions from a few unreliable data points. ~~Differences between results can be explained by 1) our study covers a longer timespan; if glacier retreat has accelerated in recent years, studies covering the last decade should exhibit comparatively greater ice loss, 2) different spatial extents and number of glaciers are covered by each respective study, 3) we use regional glacier profiles separated into 100 m elevation bands to extrapolate over regions with low image contrast, which does not capture intrinsic natural variability between glaciers, and 4) radar penetration uncertainties involved with SRTM data, which are not an issue in this study as in Kääb et al (2012) and Gardelle et al (2013).~~

Using a degree-day melt model, Rupper et al. (2012) estimated an area-averaged, net mass balance of -1.4 ± 0.6 m.w.e. yr^{-1} for the entire glacierized area (glaciers and perennial snowpack) of the Bhutanese watershed. Recently published in-situ measurements of –1.12 to –2.04 m.w.e. yr^{-1} between 2003 and 2014 for the Gangju La glacier (located approximately 15 km southwest from the toe of glacier d in Fig. 2) agree well with the melt model results (Tshering and Fujita, 2015). Compared to the remote sensing estimates, the modelled and in situ results are significantly more negative. Though difficult to compare regional changes to local ones, Cogley (2012) suggest that the discrepancy between in situ vs. remote sensing measurements may be explained by the smaller size and lower elevations of glaciers selected for fieldwork, along with unquantified local factors such as mass gain by snow avalanching. Regarding the melt model, it does not account for the insolating effects of debris-cover, while accounting for the albedo effects of the debris, which would lead to a significant overestimation of modeled melt over debris-covered glaciers. For clean ice glaciers and perennial snow, the modeled net mass balance is considerably less negative, -0.3 ± 0.2 m.w.e. yr^{-1}. This latter value is more consistent with our geodetic mass balance of -0.176 ± 0.05 m.w.e. yr^{-1} presented here, yet still on the high end. Taken together, the remote sensing data support a more conservative model scenario of future glacierized area loss and meltwater flux change, highlight the benefit of informing modeling and in-situ approaches with remote sensing, and exemplify the need for further understanding of these discrepancies.

Formatted: Superscript

Formatted: Indent: First line: 0.25"

Formatted: Indent: First line: 0"

4.2 Glacier dynamics

The elevation change maps presented in Fig. 3 reveal a variety of decadal scale glacier change patterns. Two north-flowing clean glaciers (a and b) appear to be retreating, losing ice near their toes as most simple glacier models predict. Another large north-flowing clean glacier has experienced thinning at the transition point between a steep slope and nearly flat terrain (glacier c). The downstream "piedmont" portion of the glacier spilling onto flat terrain has not thinned as much, suggesting it is dynamically decoupled from the thinning steeper glacier portion above. The thinning pattern may also be influenced by a decrease in mass flux of the smaller confluence glacier. This would result in thinning of the ice fall at the confluence, thus strengthening the disconnect between upper and lower reaches of the glacier. The observed decoupling of the "piedmont" tongue may indicate potential for the onset of proglacial lake formation, because decreasing flow velocities and increased mass losses can induce the formation and expansion of glacial lakes under favourable topographic conditions (Thakuri et al, 2015). Modelled bed overdeepenings in this region also suggest that gently sloping thick glacier tongues of these north-flowing glaciers (including glacier c) have high potential for lake formation and enlargement (Linsbauer et al, 2016). Other glaciers terminating in nearly-flat valleys have already begun to form such lakes, which can become highly hazardous due to GLOF potential. In the Lunana region for example, the proglacial lake Lugge Tsho (located at the toe of glacier i in Figs. 2 and 3) burst on 6 October 1994 resulting in the deaths of 21 persons (Watanabe and Rothacher, 1996)~~(Watanbe and Rothacher, 1996)~~.

Three large south-flowing glaciers (d, e, and f) are heavily debris-covered. Modern satellite imagery viewed in Google Earth~~Modern high-resolution satellite imagery (such as Quickbird)~~ reveal melt ponds and associated ice cliffs on the surfaces of these glaciers, which can explain their irregular downwasting patterns. Recent studies have shown a disproportionately large amount of melting occurs along exposed ice cliffs compared to debris-covered regions. Supraglacial melt ponds are formed as the ice cliffs retreat, and the ponds interact with englacial conduits to enhance melting (Immerzeel et al, 2014; Reid and Brock, 2014; Sakai and Fujita, 2010). Ice cliff formation is still not well-understood, but possible mechanisms include collapse of englacial voids (initially created by drainage of melt ponds), aspect-induced differences in solar radiation, and debris slope slumping (Benn et al, 2012). A recent grid-based model of supraglacial ice cliff backwasting on debris-covered glaciers has confirmed the importance of cliffs as contributors to total mass loss of debris-covered glaciers, and shown that melt is highly variable in space, suggesting that simple models provide inaccurate estimates of total melt volumes (Buri et al, 2015). Miles et al (2016) also showed that supraglacial ponds efficiently convey atmospheric energy to a glaciers interior, promoting the downwasting process.

Thorthormi glacier (glacier h) is a distinct example of a debris-covered calving glacier, with ice loss due to calving and thermal undercutting apparently far outweighing downwasting associated with ice cliffs and melt ponds. The largest thickness changes are occurring on the steep mid-section portion of the glacier, which may indicate a dynamic thinning response to calving as ice is lost at the glacier toe. As ice is removed from the glacier and stored in the lake, areas once covered by ice are now replaced by water, resulting in small thickness changes observed near the glacier toe. This is

consistent with observations of the rapid growth of the Thorthormi lake, which is a potential GLOF hazard (Fujita et al, 2008), and suggests that ice loss is slightly underestimated by DEM differencing methods for these calving glaciers.

Glacier k has an anomalously large ice volume loss (~0.4–5 km³), accounting for approximately 20% of the total ice volume loss of the 21 analysed glaciers. No stereo matching or georeferencing problems are apparent, and Gardelle et al (2013) show a similar large ice loss during a different timespan (1999-2011) using different elevation data (SRTM and SPOT5); thus our result is not likely due to image processing errors. It is currently unclear why this glacier has undergone such a comparatively large ice loss; however, glacier k has a large, wide accumulation area to the west (Fig. 2). One possible explanation could be that glacier thinning has caused the ice divide between glaciers k and c to shift and change position over time, thus decreasing the accumulation area and reducing the supply of ice mass for glacier k, causing a drastic reduction in volume.

4.3 Glacier types comparison

Profiles of ice thickness change vs. elevation show distinct thinning patterns for each glacier type (Fig 4). The clean-ice change profile ~~is close to zero (~~appears slightly positive~~)~~ in the accumulation zones, and thinning generally becomes ~~more negative~~greater ~~as elevation decreases~~with decreasing elevation, reaching approximately ~~-35~~ -40 m of ~~ice loss~~thinning over the 32-year timespan at 5000 m elevation, then ~~increasing~~ exhibiting less thinning near glacier toes. First, glacier k does not contribute to the lowest elevation bin, which results in smaller thickness change since glacier k is dominantly affecting the regional thinning profile (see Fig. S2). While some of the lower thinning rates may be due to insulating effects of more comprehensive debris-cover on glacier toes, we conclude that the primary factor is that the toes are thinner to begin with, and thus have less ice to lose. Our 1974 glacier outlines include glacier toes which were already thin at that time, and we expect thinning from 1974 onwards to be smaller near the toes. ~~again to ~10 m of ice loss at 4700 m elevation. This lesser rate of thinning at lowest elevations could be due in part to: 1) some insulating debris cover at glacier toes, even though these glaciers are predominately clean-ice (< 20% of glacier area is debris covered), 2) slightly inaccurate glacier outlines may include small portions of ice-free terrain near glacier toes, and 3) the total amount of thinning which can occur at glacier toes is limited compared to other parts of the glacier, simply because toes are generally thinner.~~ The debris-covered change profile starts near zero m ice loss at 5700 m elevation, ~~then decreases to approximately -10 m of ice loss at 5300 m elevation, and remains between -5 and -10 m of ice loss down to the lowest elevations~~with thinning rates increasing steadily towards lower elevations, reaching around -20 m of thinning at 4200 m. The calving-glaciers profile is somewhat erratic, fluctuating between -10 m and -50 m of ice loss from 6000 m down to 4400 m elevation, as several glaciers residing at different elevations have undergone significant ice loss due to calving.

Although elevation distributions of ice loss differ between glacier types, overall geodetic mass balance values for ~~Our results show the same order of ice loss for~~ both debris-covered and clean glacier groups ~~between 1974 and 2006~~are similar in magnitude, with overlapping uncertainties (-0.13 ± 0.06 for clean ice and -0.19 ± 0.11 m.w.e. yr^{-1} for debris-covered). This supports previous findings of similar regional averaged thinning rates between glacier types in the Himalayas over more

recent ~10-year timeframes (Kääb et al, 2012; Gardelle et al, 2013). We hypothesize that the similar magnitudes of ice loss can largely be explained by ~~different accumulation area ratios (AAR)~~contrasting glacier hypsometries. For many clean-ice glaciers, large accumulation zones reside ~~above the ELA~~at high elevations, while debris-covered glaciers tend to have small accumulation zones and thus the majority of glacier area lies ~~below the ELA~~at lower elevations. In turn, any given increase in temperature melts and thins a larger portion of debris-covered glacier area compared to clean-ice glacier area. As Fig. 4 illustrates, the magnitude of thinning for debris-covered glaciers is significantly less that for clean-ice glaciers, presumably due to insulating effects of the debris. However, integrating this smaller thinning across comparatively larger regions ~~below the ELA~~at lower elevations yields similar and even more negative mass balance values compared to the ~~uninsulated~~ clean-ice glaciers. Additionally, our measured geodetic thinning is influenced by both mass balance processes and ice dynamics (emergent velocities). Kääb et al (2005) showed that the large north-flowing clean-ice glaciers in Bhutan have flow velocities up to 200 m yr^{-1}, while south-flowing debris-covered glaciers are nearly stagnant. Thus, ice advection down-glacier is significantly greater for these clean-ice glaciers, making the apparent mass balance less negative in the ablation zones of the clean-ice glaciers as compared to the debris-covered glaciers.

Recent studies have identified relationships between glacier slope, surface velocity, and thinning rates. For example in the Langtang Himal (Nepal), ~~greater thinning is occurring at locations of low slope and~~zones with low surface flow velocities and low slopes tend to be associated ~~low surface velocit~~with ~~ty~~dynamic decay of surface features, and local accelerations in thinning for these regions correlate with development of supraglacial ice cliffs and lakes (Pellicciotti et al, 2015; Ragettli et al, 2016). ~~–~~We find a similar relationship in Bhutan, especially regarding glaciers d, e, and f, which have large, flat, debris-covered ablation zones, near-stagnant flow velocities (Kääb, 2005), and supraglacial ponds. As discussed in section 4.2, melt ponds, ice cliff dynamics, and englacial conduits likely play a significant role in enhancing melt for these glaciers. Additionally, longwave radiative flux change for a given temperature change is greater in regions at warmer temperatures. This may further enhance melt for lower elevation debris-covered glaciers; given that longwave atmospheric radiation is the most important heat source for melting of snow and ice (Ohmura, 2001).

Some glaciers in the region are partially debris-covered, with ~~heavy~~ greater proportions of debris-covered area near glacier toes, and ~~lighter~~ lower proportions of debris-covered area moving up the glacier (glaciers h and o). The mid-glacier regions with ~~lighter~~ less debris-covered area exhibit greater thinning; this may be a result of enhanced ice melt due to the albedo effect of supra-glacial debris-cover that is thin enough to not provide considerable insulation effects, and the fact that bare ice melts at a faster rate than debris-covered ice at the same elevation. Modelling studies in the Khumbu region indicate that debris-covered tongues will detach from their accumulation areas in the future, leading to greater future melt rates (Shea et al, 2015; Rowan et al, 2015).~~.~~

Calving glaciers in the study area have more negative mass balances compared to both types of land-terminating glaciers (both clean and debris-covered), and represent a disproportionately large amount of the total ice volume loss relative to their aerial extent. For these glaciers, large moraine-dammed lakes have formed as a result of expansion and merging of smaller supraglacial lakes, and glacial meltwater is effectively stored adjacent to glacier termini (Basnett et al, 2013). As changing

climate increases glacier melt, the resulting lakes interact with remaining ice to further enhance melt through thermal undercutting processes independent of climate (Sakai et al, 2009; Thompson et al, 2012). This positive feedback mechanism has important implications for future hazard and water resource issues, especially for glaciers terminating in flat valleys with potential lake-forming topographies. Gardelle (2011) estimated that in the eastern HKH (India, Nepal, and Bhutan) glacial lakes have grown continuously between 1990 and 2009 by 20% to 65%. Thus, these glacier-lake systems not only represent GLOF hazards, but will likely play a key role in the Himalayan ice mass budget during the coming decades.

5 Conclusions

We applied a new DEM extraction pipeline toward Hexagon spy satellite imagery and ASTER data to compute glacier thickness changes over a multi-decadal timescale across a large glacierized area (~365 ~~27~~ km^2) in the eastern Himalayas. The consistency of the DEM extraction method provided high geolocational accuracy and minimized elevation biases when differencing the DEMs. In addition, the long timespan (1974-2006) allowed for effective separation of glacier change from noise inherent in the remote sensing methods. Results provide insight into the complex dynamics of glaciers in the monsoonal Himalayas, and highlight similarities and differences in the decadal responses of clean, debris-covered, and calving glaciers. Though regional thinning and ice loss is apparent, individual glacier dynamics vary widely depending on elevation, hypsometry, extent and thickness of debris, and potential for calving in proglacial lakes. Both clean and debris-covered glaciers show similar negative geodetic mass balances, while lake-terminating glaciers have geodetic mass balances more negative than land-terminating glaciers. The more negative mass balances of lake-terminating glaciers suggests that calving and thermal undercutting are important mechanisms contributing to ice loss in the region, and highlights the rapidly growing hazard potential of GLOFs in the monsoonal Himalayas. Overall, these results enhance understanding regarding potential glacier contribution to sea-level rise, impact on hydrological resources, and hazard potential for high mountain regions and downstream populations in Asia.

Acknowledgements. This work was funded by NSF Grants 1256551 and 1304397 to SR, and a Rocky Mountain NASA Space Grant Consortium (RMNSGC) fellowship to JM. JMS acknowledges support by the NSF Grant EAR-1304351 and by the Lamont Climate Center. We thank the USGS, NASA, and Japan Space Systems for providing access to Hexagon and ASTER data, and gratefully acknowledge Barry Bickmore and Jani Radebaugh for constructive comments on the manuscript.

References

Abrams, M., The Advanced Spaceborne Thermal Emission and Reflection Radiometer (ASTER): data products for the high spatial resolution imager on NASA's Terra platform: International Journal of Remote Sensing, v. 21, p. 847-859, 2000.

Bajracharya, S.R., Maharjan, S.B., and Shrestha, F., The status and decadal change of glaciers in Bhutan from the 1980s to 2010 based on satellite data: Annals of Glaciology, v. 55, p. 159-166, 2014.

Basnett, S., Kulkarni, A.V., and Bolch, T., The influence of debris cover and glacial lakes on the recession of glaciers in Sikkim Himalaya, India: Journal of Glaciology, v. 59, p. 1035-1046, 2013.

Bay, H., Tuytelaars, T., and Van Gool, L., Anonymous Surf: Speeded up robust features: Springer, p. 404-417, 2006.

Beldring, S., and VoksØ, A., Climate Change Impact on Flow Regimes of Rivers in Bhutan and Possible Consequences for Hydropower Development: Hydro Nepal: Journal of Water, Energy and Environment, v. 11, p. 67-68, 2012.

Benn, D., Bolch, T., Hands, K., Gulley, J., Luckman, A., Nicholson, L., Quincey, D., Thompson, S., Toumi, R., and Wiseman, S., Response of debris-covered glaciers in the Mount Everest region to recent warming, and implications for outburst flood hazards: Earth-Science Reviews, v. 114, p. 156-174, 2012.

Berthier, E., Arnaud, Y., Kumar, R., Ahmad, S., Wagnon, P., and Chevallier, P., Remote sensing estimates of glacier mass balances in the Himachal Pradesh (Western Himalaya, India): Remote Sensing of Environment, v. 108, p. 327-338, 2007.

Bhambri, R., Bolch, T., Kawishwar, P., Dobhal, D., Srivastava, D., and Pratap, B., Heterogeneity in glacier response in the upper Shyok valley, northeast Karakoram: The Cryosphere, v. 7, p. 1385-1398, 2013.

Bolch, T., Pieczonka, T., and Benn, D., Multi-decadal mass loss of glaciers in the Everest area (Nepal Himalaya) derived from stereo imagery: The Cryosphere, v. 5, p. 349-358, 2011.

Bolch, T., Kulkarni, A., Kaab, A., Huggel, C., Paul, F., Cogley, J.G., Frey, H., Kargel, J.S., Fujita, K., Scheel, M., Bajracharya, S., and Stoffel, M., The state and fate of Himalayan glaciers: Science, v. 336, p. 310-314, 2012.

Buri, P., Pellicciotti, F., Steiner, J.F., Miles, E.S., and Immerzeel, W.W., A grid-based model of backwasting of supraglacial ice cliffs on debris-covered glaciers: Annals of Glaciology, 2015.

Cogley, J.G., Climate science: Himalayan glaciers in the balance: Nature, v. 488, p. 468-469, 2012.

Curran, P.J., The semivariogram in remote sensing: an introduction: Remote Sensing of Environment, v. 24, p. 493-507, 1988.

Fujita, K., Suzuki, R., Nuimura, T., and Sakai, A., Performance of ASTER and SRTM DEMs, and their potential for assessing glacial lakes in the Lunana region, Bhutan Himalaya: Journal of Glaciology, v. 54, p. 220-228, 2008.

Fusiello, A., and Irsara, L., Quasi-euclidean uncalibrated epipolar rectification, Pattern Recognition, 2008. ICPR 2008. 19th International Conference on, , p. 1-4, 2008.

Gardelle, J., Arnaud, Y., and Berthier, E., Contrasted evolution of glacial lakes along the Hindu Kush Himalaya mountain range between 1990 and 2009: Global and Planetary Change, v. 75, p. 47-55, 2011.

Gardelle, J., Berthier, E., and Arnaud, Y., Impact of resolution and radar penetration on glacier elevation changes computed from DEM differencing: Journal of Glaciology, v. 58, p. 419-422, 2012.

Gardelle, J., Berthier, E., Arnaud, Y., and Kaab, A., Region-wide glacier mass balances over the Pamir-Karakoram-Himalaya during 1999-2011: Cryosphere, v. 7, p. 1885-1886, 2013.

Hartley, R., and Zisserman, A., Anonymous Multiple view geometry in computer vision: Cambridge university press, 2003.

Hirschmüller, H., Stereo processing by semiglobal matching and mutual information: Pattern Analysis and Machine Intelligence, IEEE Transactions On, v. 30, p. 328-341, 2008.

Holzer, N., Vijay, S., Yao, T., Xu, B., Buchroithner, M., and Bolch, T., Four decades of glacier variations at Muztagh Ata (eastern Pamir): a multi-sensor study including Hexagon KH-9 and Pléiades data: The Cryosphere, v. 9, p. 2071-2088, 2015.

Huss, M., Density assumptions for converting geodetic glacier volume change to mass change: The Cryosphere, v. 7, p. 877-887, 2013.

Immerzeel, W., Kraaijenbrink, P., Shea, J., Shrestha, A., Pellicciotti, F., Bierkens, M., and De Jong, S., High-resolution monitoring of Himalayan glacier dynamics using unmanned aerial vehicles: Remote Sensing of Environment, v. 150, p. 93-103, 2014.

Immerzeel, W.W., van Beek, L.P., and Bierkens, M.F., Climate change will affect the Asian water towers: Science, v. 328, p. 1382-1385, 2010.

Kääb, A., Combination of SRTM3 and repeat ASTER data for deriving alpine glacier flow velocities in the Bhutan Himalaya: Remote Sensing of Environment, v. 94, p. 463-474, 2005.

Kääb, A., Berthier, E., Nuth, C., Gardelle, J., and Arnaud, Y., Contrasting patterns of early twenty-first-century glacier mass change in the Himalayas: Nature, v. 488, p. 495-498, 2012.

Kim, T., A study on the epipolarity of linear pushbroom images: Photogrammetric Engineering and Remote Sensing, v. 66, p. 961-966, 2000.

Lamsal, D., Sawagaki, T., and Watanabe, T., Digital terrain modelling using Corona and ALOS PRISM data to investigate the distal part of Imja Glacier, Khumbu Himal, Nepal: Journal of Mountain Science, v. 8, p. 390-402, 2011.

Linsbauer, A., Frey, H., Haeberli, W., Machguth, H., Azam, M., and Allen, S., Modelling glacier-bed overdeepenings and possible future lakes for the glaciers in the Himalaya–Karakoram region: Annals of Glaciology, v. 57, p. 119, 2016.

Mattar, K.E., Vachon, P.W., Geudtner, D., Gray, A.L., Cumming, I.G., and Brugman, M., Validation of alpine glacier velocity measurements using ERS tandem-mission SAR data: IEEE Transactions on Geoscience and Remote Sensing, v. 36, p. 974-984, 1998.

Maurer, J., and Rupper, S., Tapping into the Hexagon spy imagery database: A new automated pipeline for geomorphic change detection: ISPRS Journal of Photogrammetry and Remote Sensing, v. 108, p. 113-127, 2015.

Miles, E.S., Pellicciotti, F., Willis, I.C., Steiner, J.F., Buri, P., and Arnold, N.S., Refined energy-balance modelling of a supraglacial pond, Langtang Khola, Nepal: Annals of Glaciology, v. 57, p. 29, 2016.

Nuth, C., and Kääb, A., Co-registration and bias corrections of satellite elevation data sets for quantifying glacier thickness change: The Cryosphere, v. 5, p. 271-290, 2011.

Nuth, C., Moholdt, G., Kohler, J., Hagen, J.O., and Kääb, A., Svalbard glacier elevation changes and contribution to sea level rise: Journal of Geophysical Research: Earth Surface, v. 115, 2010.

Oder, F.C., Fitzpatrick, J.C., and Worthman, P.E., Anonymous The HEXAGON Story: Center for the Study of National Reconnaissance, 2012.

Ohmura, A., Physical basis for the temperature-based melt-index method: Journal of Applied Meteorology, v. 40, p. 753-761, 2001.

Paul, F., Evaluation of different methods for glacier mapping using Landsat TM, Proceedings, EARSeL-SIG Workshop, 2000.

Pellicciotti, F., Stephan, C., Miles, E., Herreid, S., Immerzeel, W.W., and Bolch, T., Mass-balance changes of the debris-covered glaciers in the Langtang Himal, Nepal, from 1974 to 1999: Journal of Glaciology, v. 61, p. 373-386, 2015.

Pellikka, P., and Rees, W.G., Anonymous Remote sensing of glaciers: techniques for topographic, spatial and thematic mapping of glaciers: CRC Press, 2009.

Pieczonka, T., Bolch, T., Junfeng, W., and Shiyin, L., Heterogeneous mass loss of glaciers in the Aksu-Tarim Catchment (Central Tien Shan) revealed by 1976 KH-9 Hexagon and 2009 SPOT-5 stereo imagery: Remote Sensing of Environment, v. 130, p. 233-244, 2013.

Pieczonka, T., and Bolch, T., Region-wide glacier mass budgets and area changes for the Central Tien Shan between~ 1975 and 1999 using Hexagon KH-9 imagery: Global and Planetary Change, v. 128, p. 1-13, 2015.

Racoviteanu, A., Arnaud, Y., Williams, M., and Manley, W., Spatial patterns in glacier characteristics and area changes from 1962 to 2006 in the Kanchenjunga–Sikkim area, eastern Himalaya: The Cryosphere, v. 9, p. 505-523, 2014.

Ragettli, S., Bolch, T., and Pellicciotti, F., Heterogeneous glacier thinning patterns over the last 40 years in Langtang Himal: The Cryosphere Discussions, v. 2016, p. 1-53, 2016.

Raj, K.B.G., Remya, S., and Kumar, K.V., Remote sensing-based hazard assessment of glacial lakes in Sikkim Himalaya: Current Science(Bangalore), v. 104, p. 359-364, 2013.

Reid, T., and Brock, B., Assessing ice-cliff backwasting and its contribution to total ablation of debris-covered Miage glacier, Mont Blanc massif, Italy: Journal of Glaciology, v. 60, p. 3-13, 2014.

Richardson, S.D., and Reynolds, J.M., An overview of glacial hazards in the Himalayas: Quaternary International, v. 65, p. 31-47, 2000.

Rolstad, C., Haug, T., and Denby, B., Spatially integrated geodetic glacier mass balance and its uncertainty based on geostatistical analysis: application to the western Svartisen ice cap, Norway: Journal of Glaciology, v. 55, p. 666-680, 2009.

Rowan, A.V., Egholm, D.L., Quincey, D.J., and Glasser, N.F., Modelling the feedbacks between mass balance, ice flow and debris transport to predict the response to climate change of debris-covered glaciers in the Himalaya: Earth and Planetary Science Letters, v. 430, p. 427-438, 2015.

Rupper, S., and Roe, G., Glacier changes and regional climate: a mass and Energy balance approach: Journal of Climate, v. 21, p. 5384-5401, 2008.

Rupper, S., Schaefer, J.M., Burgener, L.K., Koenig, L.S., Tsering, K., and Cook, E.R., Sensitivity and response of Bhutanese glaciers to atmospheric warming: Geophysical Research Letters, v. 39, 2012.

Sakai, A., Nishimura, K., Kadota, T., and Takeuchi, N., Onset of calving at supraglacial lakes on debris-covered glaciers of the Nepal Himalaya: Journal of Glaciology, v. 55, p. 909-917, 2009.

Sakai, A., and Fujita, K., Formation conditions of supraglacial lakes on debris-covered glaciers in the Himalaya: Journal of Glaciology, p. 177-181, 2010.

Scherler, D., Bookhagen, B., and Strecker, M.R., Spatially variable response of Himalayan glaciers to climate change affected by debris cover: Nature Geoscience, v. 4, p. 156-159, 2011.

Shea, J., Immerzeel, W., Wagnon, P., Vincent, C., and Bajracharya, S., Modelling glacier change in the Everest region, Nepal Himalaya: The Cryosphere, v. 9, p. 1105-1128, 2015.

Strozzi, T., Luckman, A., Murray, T., Wegmuller, U., and Werner, C.L., Glacier motion estimation using SAR offset-tracking procedures: IEEE Transactions on Geoscience and Remote Sensing, v. 40, p. 2384-2391, 2002.

Surazakov, A., and Aizen, V., Positional accuracy evaluation of declassified Hexagon KH-9 mapping camera imagery: Photogrammetric Engineering & Remote Sensing, v. 76, p. 603-608, 2010.

Thakuri, S., Salerno, F., Bolch, T., Guyennon, N., and Tartari, G., Factors controlling the accelerated expansion of Imja Lake, Mount Everest region, Nepal: Annals of Glaciology, 2015.

Thompson, S.S., Benn, D.I., Dennis, K., and Luckman, A., A rapidly growing moraine-dammed glacial lake on Ngozumpa Glacier, Nepal: Geomorphology, v. 145, p. 1-11, 2012.

Tshering, P., and Fujita, K., First in situ record of decadal glacier mass balance (2003–2014) from the Bhutan Himalaya: Annals of Glaciology, 2015.

Watanabe, T., and Rothacher, D., The 1994 Lugge Tsho glacial lake outburst flood, Bhutan Himalaya: Mountain Research and Development, p. 77-81, 1996.

Williams, M.W., Wilson, A., Tshering, D., Thapa, P., and Kayastha, R.B., Using geochemical and isotopic chemistry to evaluate glacier melt contributions to the Chamkar Chhu (river), Bhutan: Annals of Glaciology, 2015.

Zemp, M., Hoelzle, M., and Haeberli, W., Six decades of glacier mass-balance observations: a review of the worldwide monitoring network: Annals of Glaciology, v. 50, p. 101-111, 2009.

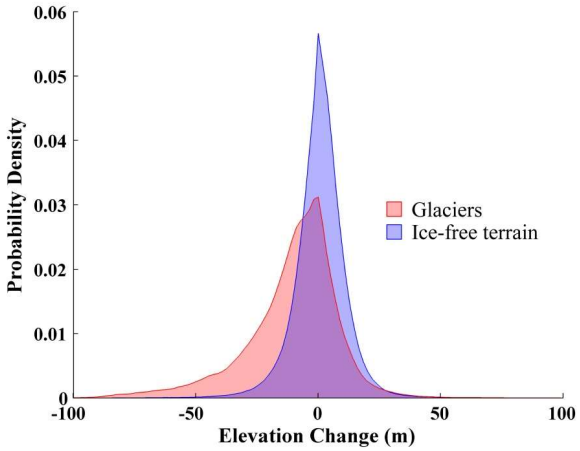

Figure 1. Probability density distributions for all pixels in the 2006 minus 1974 elevation change maps obtained via DEM differencing, separated into glacial ice terrain and surrounding ice-free terrain groups. The glacial terrain distribution has mean = -10.9 m, median = -7.3 m, and σ = 19.7 m. By comparison, the ice-free terrain distribution has mean = 0.7 m, median = 0.9 m, and σ = 10.9 m. Non-zero elevation changes in the ice-free terrain distribution are likely caused by a combination of actual changes such as landslides, along with intrinsic elevation error associated with stereo photogrammetric methods used to create the DEMs.

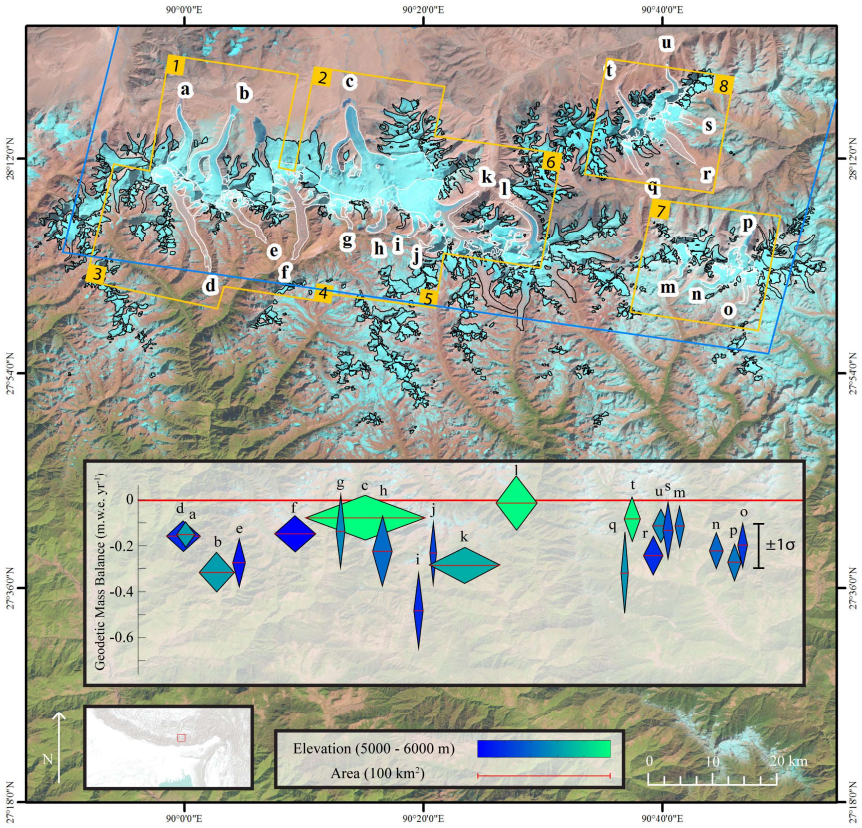

Figure 2. Landsat 8 image showing study region located in the eastern Himalayas and Tibetan Plateau. Black outlines identify all glaciers in the region, while white outlines denote glaciers used in this study, identified by letters a-u. Glacier outlines were downloaded from the ICIMOD mountain geoportal. Orange outlines indicated extent of extracted 1974 Hexagon DEMs; blue line indicates extent of the 2006 ASTER DEM. Inset: Annual gGeodetic mass balances for selected glaciers during the 1974 to 2006 period (2006 ASTER DEM minus 1974 Hexagon DEMs), where each diamond represents a glacier. Central red lines are geodetic mass balances for each glacier in m.w.e. yr_a^{-1} (meters water equivalent per year). Diamond widths are proportional to total glacier area, heights indicate ±1 standard error (SEM) uncertainty, and colors specify mean glacier elevations. Thick red line indicates zero change.

Formatted: Superscript

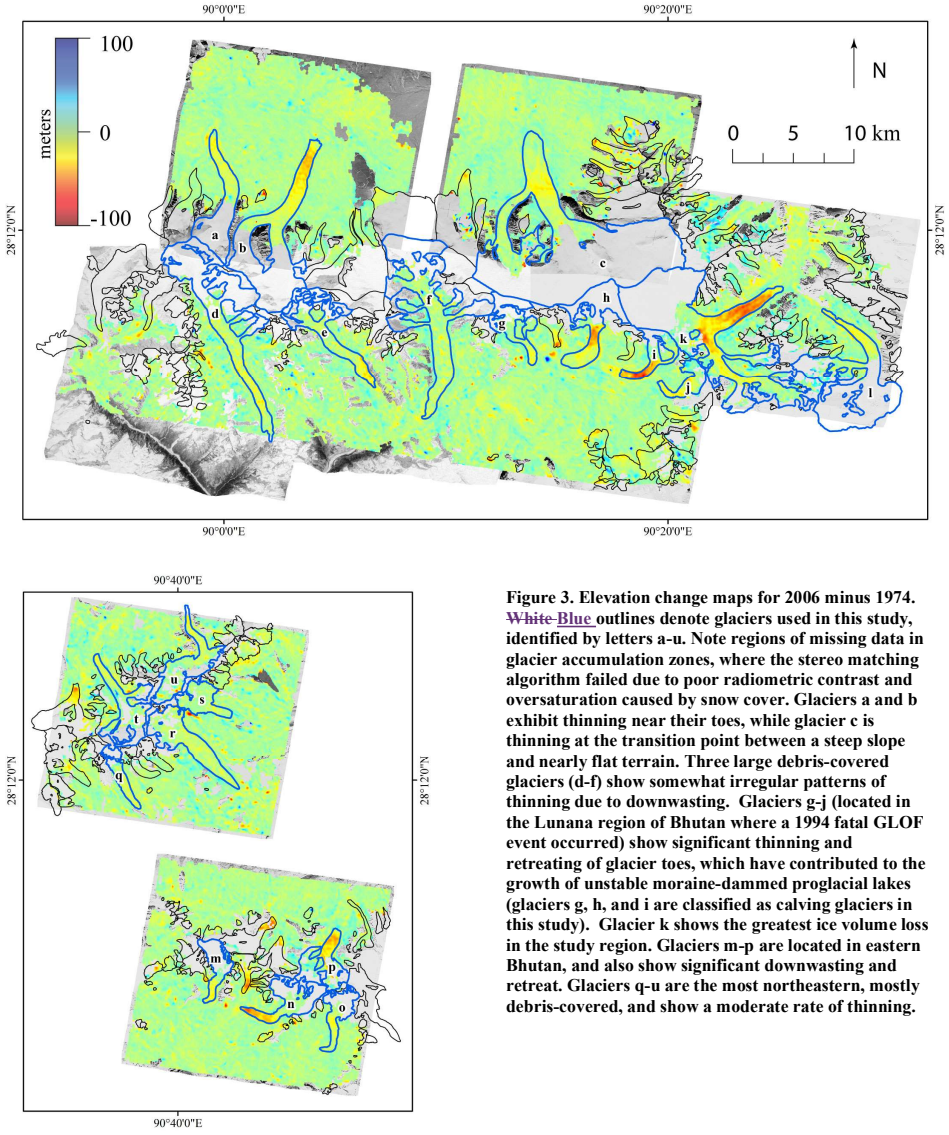

Figure 3. Elevation change maps for 2006 minus 1974. ~~White~~ Blue outlines denote glaciers used in this study, identified by letters a-u. Note regions of missing data in glacier accumulation zones, where the stereo matching algorithm failed due to poor radiometric contrast and oversaturation caused by snow cover. Glaciers a and b exhibit thinning near their toes, while glacier c is thinning at the transition point between a steep slope and nearly flat terrain. Three large debris-covered glaciers (d-f) show somewhat irregular patterns of thinning due to downwasting. Glaciers g-j (located in the Lunana region of Bhutan where a 1994 fatal GLOF event occurred) show significant thinning and retreating of glacier toes, which have contributed to the growth of unstable moraine-dammed proglacial lakes (glaciers g, h, and i are classified as calving glaciers in this study). Glacier k shows the greatest ice volume loss in the study region. Glaciers m-p are located in eastern Bhutan, and also show significant downwasting and retreat. Glaciers q-u are the most northeastern, mostly debris-covered, and show a moderate rate of thinning.

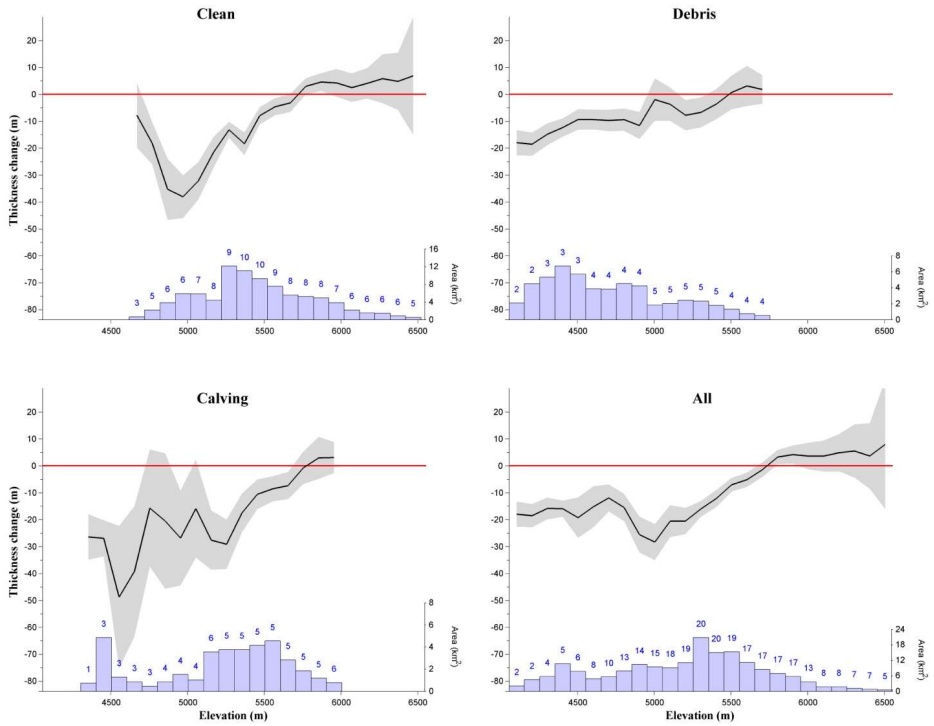

Figure 4. Ice thickness change profiles for clean ice, debris covered, calving, and all glaciers (rates of change can be obtained by dividing values on the vertical axis by 32 years). ~~Elevation~~ Thickness change pixels are separated into 100 m bands; black lines are the mean, and the grey shaded regions represent the standard error of the mean estimated as $\sigma_z/\sqrt{n_z}$, where σ_z is the standard deviation of elevation change for each band and n_z is calculated using Eq. 5. The glacier area (km²) contained in each band is indicated by the blue histogram bars, and the number of glaciers contributing to each elevation band is shown by the blue number above each bin. Note that the histogram bars do not include extrapolated data.

Supplement

Table S1. Vertical accuracy statistics[a] of Hexagon DEMs relative to the 2006 ASTER DEM (meters)

ID	Lon	Lat[b]	$RMSE_z$	Mean	Median	NMAD[c]	STD	68.3%Q	95%Q
1	90.05	28.25	8.1	0.5	0.7	6.4	8.1	6.8	15.9
2	90.26	28.24	8.6	1.2	1.3	7.3	8.5	7.5	15.6
3	89.97	28.09	11.5	1.4	1.4	8.7	11.5	9.4	22.5
4	90.12	28.10	11.6	0.7	0.8	9.2	11.6	9.8	21.9
5	90.27	28.08	12.8	0.6	1.0	8.7	12.8	9.4	24.4
6	90.42	28.14	14.9	1.6	1.5	11.6	14.8	12.7	30.3
7	90.73	28.05	8.9	0.1	0.6	6.6	8.9	7.0	17.8
8	90.66	28.25	11.8	0.4	1.1	8.9	11.8	9.5	22.5

[a] Over assumed stable terrain (i.e. excluding glaciers). [b] Center of each Hexagon DEM region.
[c] Normalized median absolute deviation. [d] Hole interpolation max area (km^2).

Formatted Table

Table S2. Glacier Change Statistics

Glacier ID	a	b	c	d	e	f	g
Longitude (deg)	89.99	90.04	90.25	89.99	90.07	90.15	90.21
Latitude (deg)	28.21	28.18	28.19	28.16	28.14	28.16	28.13
Mean Elevation (m)	5710	5712	6183	4940	4565	4853	5012
1974 Area (km^2)	13.4 ± 1.3	25.0 ± 2.5	86.2 ± 8.6	23.5 ± 2.3	8.8 ± 0.9	30.1 ± 3.0	5.4 ± 0.5
ΔV (km^3)	-0.08 ± 0.03	-0.29 ± 0.07	-0.26 ± 0.31	-0.14 ± 0.06	-0.09 ± 0.03	-0.17 ± 0.09	-0.03 ± 0.03
ΔV_{extrap} (km^3)	-0.05 ± 0.03	-0.27 ± 0.07	0.09 ± 0.31	-0.20 ± 0.06	-0.09 ± 0.03	-0.18 ± 0.09	-0.03 ± 0.03
$\bar{h}$ (m)	-5.6 ± 2.2	-12.0 ± 3.2	-3.0 ± 3.6	-6.1 ± 2.5	-10.3 ± 4.0	-5.5 ± 2.9	-5.2 ± 5.9
$\dot{b}$ (m.w.e.)	-0.15 ± 0.06	-0.32 ± 0.09	-0.08 ± 0.10	-0.16 ± 0.07	-0.27 ± 0.11	-0.15 ± 0.08	-0.14 ± 0.16
Data coverage (%)	39	48	28	49	100	68	100
Debris coverage (%)	1	6	3	41	37	44	16
Calving (y/n)	n	y	n	n	n	n	y

h	i	j	k	l	m	n
90.27	90.33	90.35	90.39	90.47	90.7	90.75
28.13	28.11	28.09	28.1	28.08	28.06	28.04
5486	5151	5154	5749	6133	5505	5450
13.8 ± 1.4	6.1 ± 0.6	5.0 ± 0.5	49.8 ± 5.0	29.7 ± 3.0	5.7 ± 0.6	9.2 ± 0.9
-0.12 ± 0.08	-0.10 ± 0.03	-0.04 ± 0.02	-0.52 ± 0.13	-0.02 ± 0.13	-0.02 ± 0.02	-0.08 ± 0.03
-0.16 ± 0.08	-0.10 ± 0.03	-0.08 ± 0.02	-0.45 ± 0.13	0.07 ± 0.13	-0.02 ± 0.02	-0.09 ± 0.03
-8.5 ± 5.7	-18.3 ± 6.0	-8.7 ± 4.8	-10.7 ± 2.8	-0.6 ± 4.3	-4.4 ± 3.3	-8.4 ± 3.1
-0.23 ± 0.15	-0.48 ± 0.16	-0.23 ± 0.13	-0.28 ± 0.08	-0.02 ± 0.11	-0.12 ± 0.09	-0.22 ± 0.08
30	100	58	54	26	60	76
17	11	10	11	14	1	1
y	y	n	n	n	n	y

o	p	q	r	s	t	u
90.79	90.78	90.62	90.66	90.68	90.63	90.67
28.03	28.06	28.21	28.24	28.26	28.25	28.29
5216	5540	5342	5139	5304	6034	5602
5.7 ± 0.6	9.1 ± 0.9	3.1 ± 0.3	12.5 ± 1.3	6.5 ± 0.7	9.8 ± 1.0	10.2 ± 1.0
-0.04 ± 0.02	-0.09 ± 0.02	-0.04 ± 0.02	-0.11 ± 0.04	-0.03 ± 0.03	-0.03 ± 0.03	-0.04 ± 0.03
-0.07 ± 0.02	-0.12 ± 0.02	-0.04 ± 0.02	-0.11 ± 0.04	-0.03 ± 0.03	-0.01 ± 0.03	-0.05 ± 0.03
-7.6 ± 3.4	-10.1 ± 3.0	-11.9 ± 6.4	-9.1 ± 3.1	-5.1 ± 4.4	-3.2 ± 3.4	-4.3 ± 2.9
-0.20 ± 0.09	-0.27 ± 0.08	-0.32 ± 0.17	-0.24 ± 0.09	-0.13 ± 0.12	-0.08 ± 0.09	-0.11 ± 0.08
63	41	100	84	100	55	51
8	1	42	39	1	19	9
n	y	n	n	n	n	n

ΔV is ice volume change without extrapolation, ΔV_{extrap} is ice volume change ~~with~~ after extrapolating missing data using regional data from individual elevation bands~~on~~. $\bar{h}$ is the spatially-averaged elevation change of the glacier ~~(after extrapolation)~~, and $\dot{b}$ is the geodetic mass balance for each glacier over the 32-year timespan ~~(after extrapolation)~~.

Table S3

	clean	debris	calving	all
Area (km^2)	221 ± 11	78 ± 4	66 ± 3	365 ± 12
Area (%)	61	21	18	
	Assuming zero change for missing data			
ΔV (km^3)	-1.09 ± 0.4	-0.55 ± 0.4	-0.70 ± 0.3	-2.34 ± 0.6
ΔV (%)	46	24	30	
$\dot{b}$ (m.w.e. yr^{-1})	-0.13 ± 0.06	-0.19 ± 0.11	-0.28 ± 0.10	-0.17 ± 0.05
	Extrapolating missing data using regional profiles			
ΔV (km^3)	-0.60 ± 0.4	-0.62 ± 0.4	-0.77 ± 0.3	-1.99 ± 0.6
ΔV (%)	30	31	39	
$\dot{b}$ (m.w.e. yr^{-1})	-0.07 ± 0.06	-0.21 ± 0.11	-0.31 ± 0.10	-0.14 ± 0.05
	Assuming zero change for missing data in glacier c, extrapolating missing data for all other glaciers			
ΔV (km^3)	-0.95 ± 0.4	-0.62 ± 0.4	-0.77 ± 0.3	-2.34 ± 0.6
ΔV (%)	41	26	33	
$\dot{b}$ (m.w.e. yr^{-1})	-0.11 ± 0.06	-0.21 ± 0.11	-0.31 ± 0.10	-0.17 ± 0.05

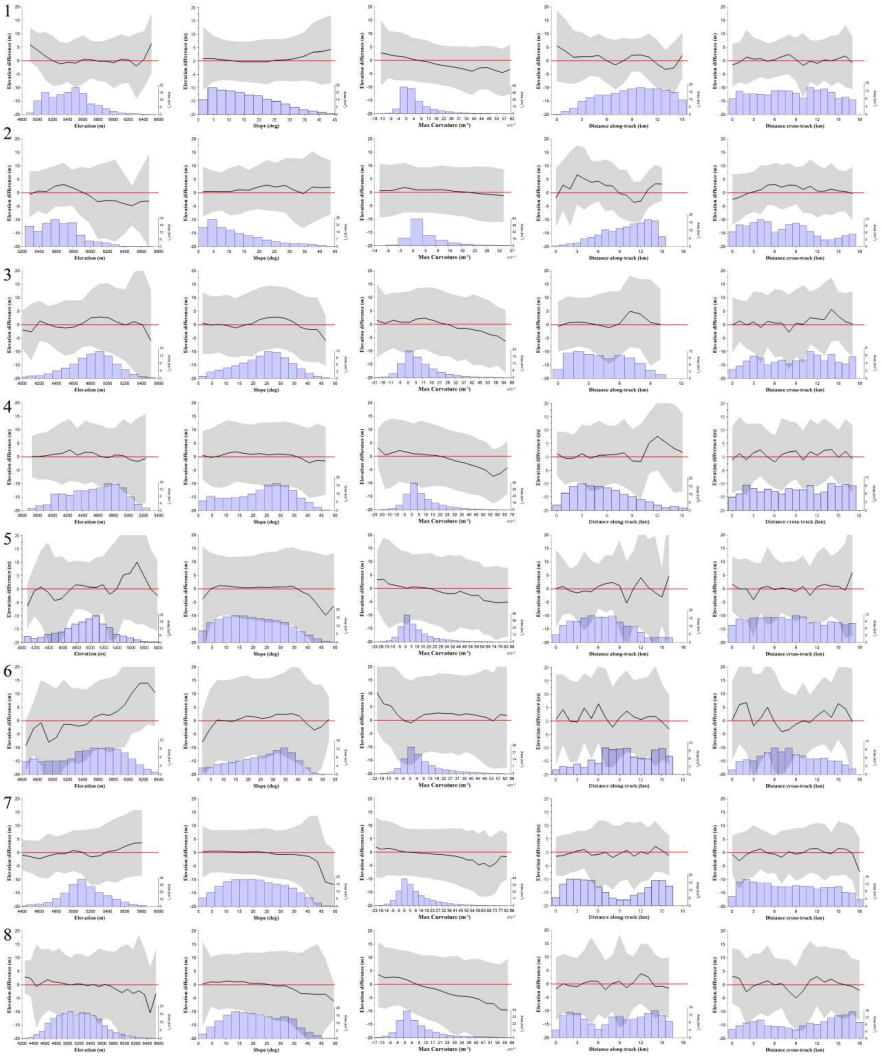

Figure S1. Plots of elevation change vs. elevation, slope, maximum curvature, and ASTER along-track and cross-track directions for assumed stable terrain in each of the 8 Hexagon DEM regions given in Table S1. Black curves and grey shaded regions indicate the mean and standard deviation of each bin, respectively. The area (km^2) contained in each bin is indicated by the blue histogram bars, calculated as the number of pixels per bin * pixel resolution^2.

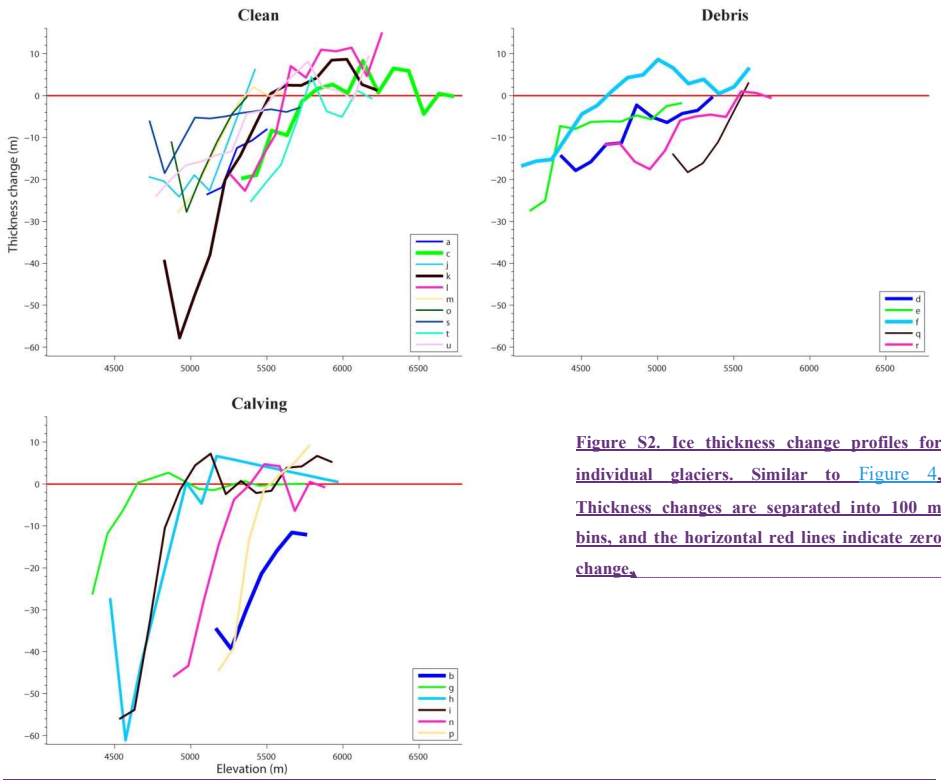

Figure S2. Ice thickness change profiles for individual glaciers. Similar to Figure 4, Thickness changes are separated into 100 m bins, and the horizontal red lines indicate zero change.

Formatted: Normal

Formatted: Font: 9 pt, Bold

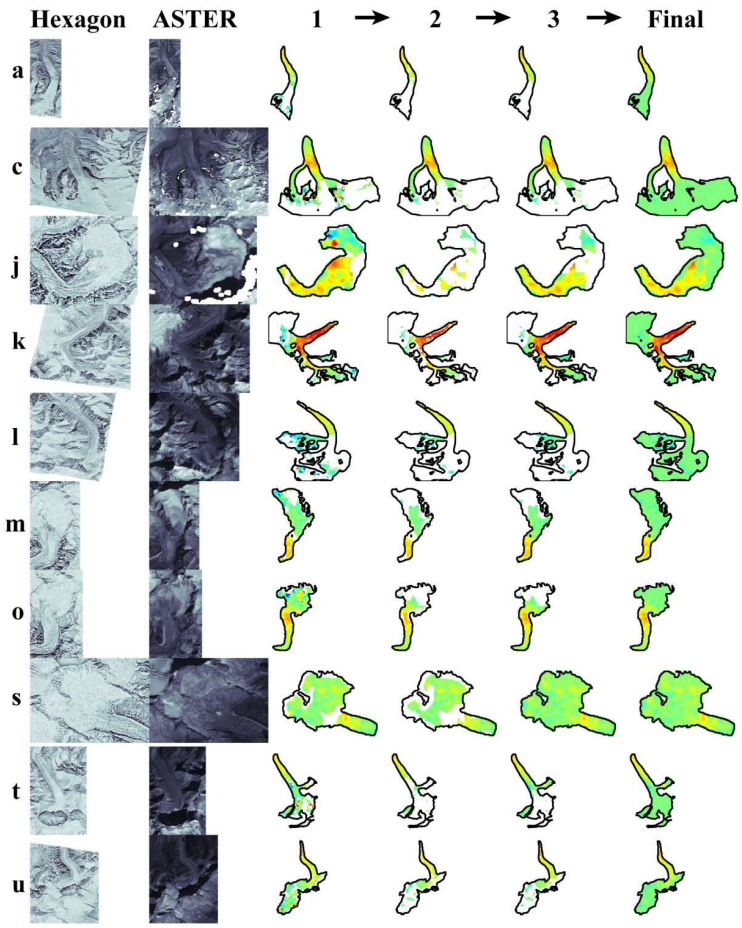

Figure S3. Hexagon and ASTER images, along with thickness change map processing stages for clean ice glaciers. Stage 1: raw elevation change maps; stage 2: after excluding erroneous pixels (see section 2.3), stage 3: after interpolating gaps smaller than 2 km^2, and stage 4: after filling remaining accumulation zone gaps with zero elevation change.

Formatted: Keep with next

Formatted: Caption

Formatted: Superscript

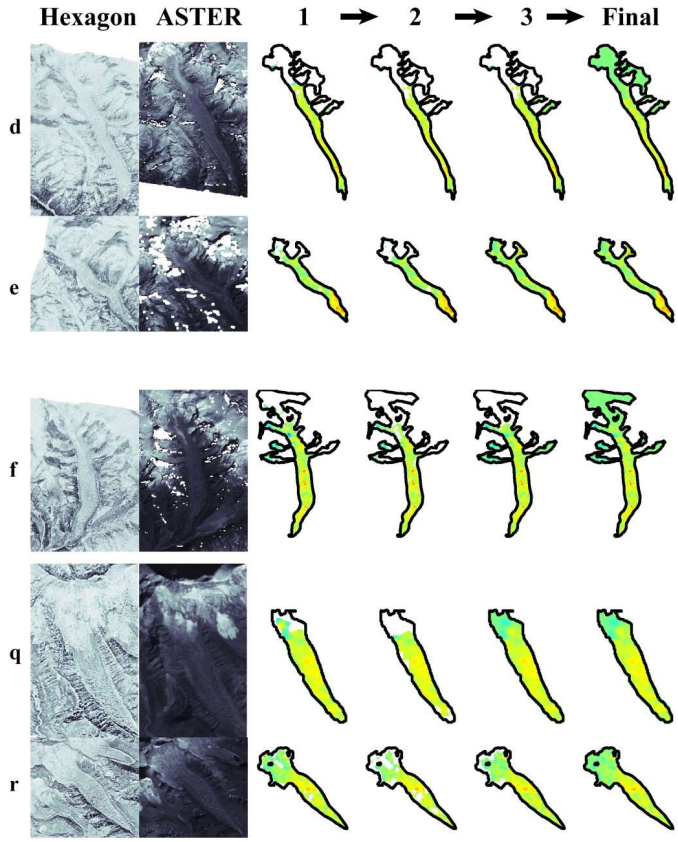

Figure S4. Same as Fig. S3, but for debris-covered glaciers.

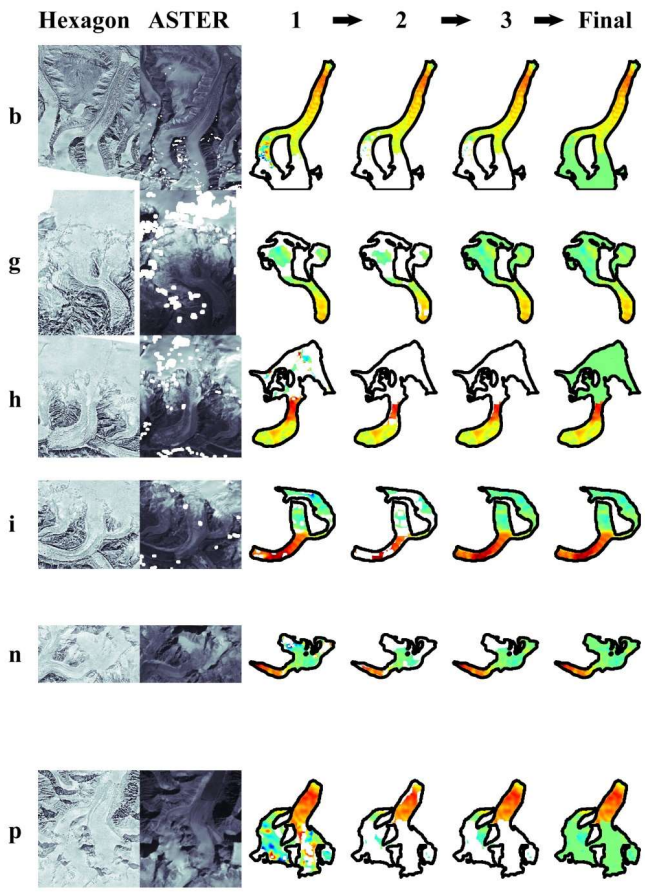

Figure S5. Same as Fig. S3, but for calving glaciers.

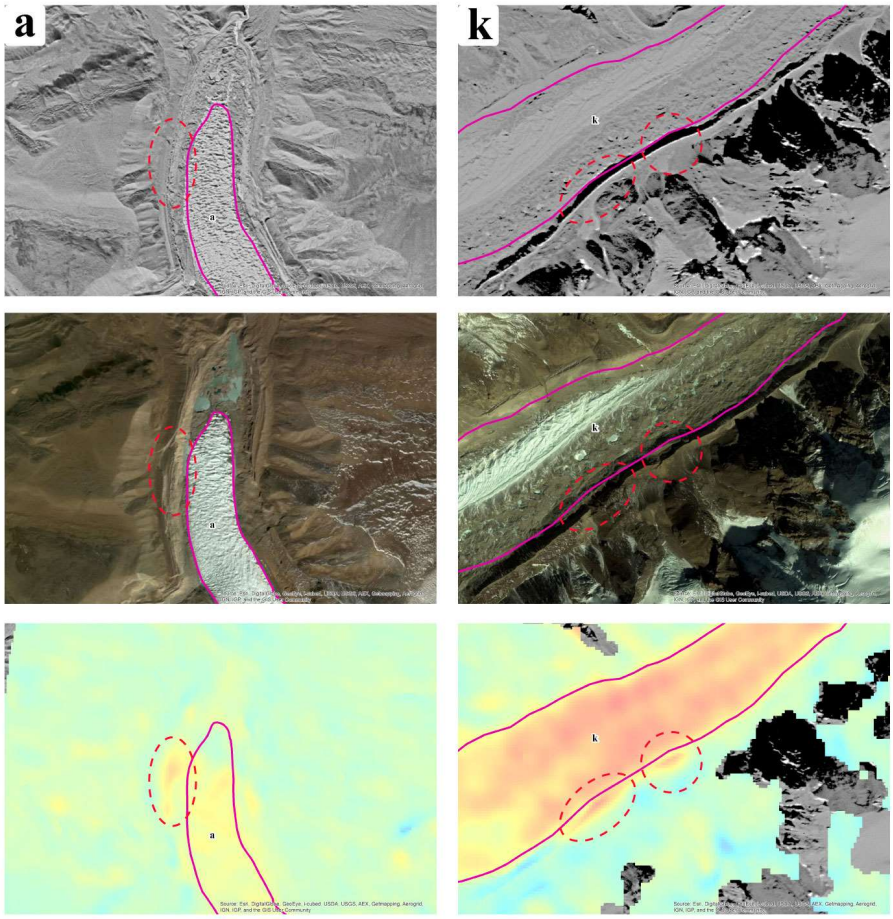

Figure S6. Two examples of unstable moraine ridges. Red dotted ellipses indicate sections which have collapsed near glaciers a and k.

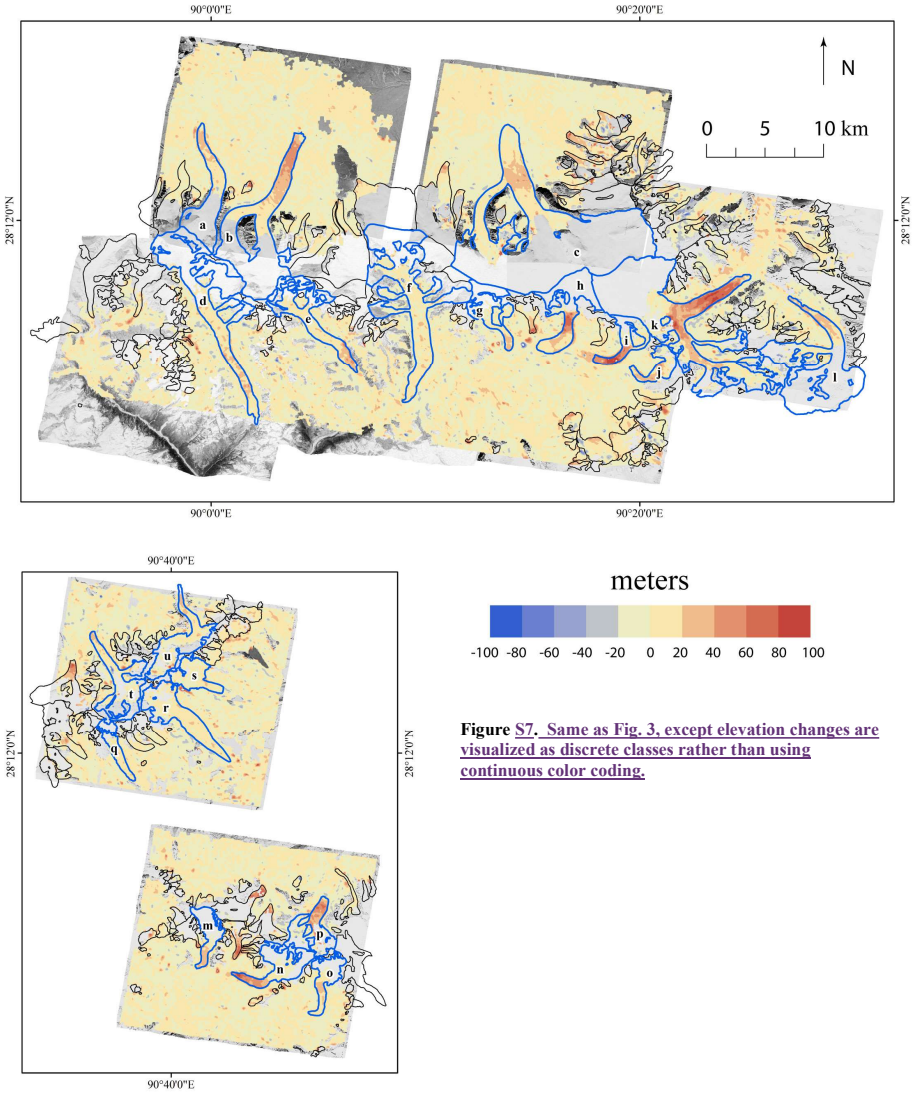

Figure S7. Same as Fig. 3, except elevation changes are visualized as discrete classes rather than using continuous color coding.